

FASHI: An untargeted survey of the 21 cm HI absorption galaxies with FASTCHUAN-PENG ZHANG,^{1,2} MING ZHU,^{1,2} PENG JIANG,^{1,2} CHENG CHENG,³ JIN-LONG XU,^{1,2} NAI-PING YU,^{1,2}
XIAO-LAN LIU,^{1,2} AND BO ZHANG^{1,2}¹*National Astronomical Observatories, Chinese Academy of Sciences, Beijing 100101, China*²*Guizhou Radio Astronomical Observatory, Guizhou University, Guiyang 550000, China*³*Chinese Academy of Sciences South America Center for Astronomy, National Astronomical Observatories, CAS, Beijing 100101, China*

ABSTRACT

The **FAST All Sky HI** survey (FASHI) will cover the entire observable sky (~ 22000 square degrees) with the Five-hundred-meter Aperture Spherical radio Telescope (FAST). With the currently released data, we perform an untargeted survey of 21 cm HI absorption galaxies at redshift $z \lesssim 0.09$ over an area of about 10000 square degrees. We have detected 51 HI absorbers, including 21 previously known and 30 new ones. The probability of occurrence for the HI absorbers in all HI galaxies is 1/1078. The radio flux densities of the FASHI absorbers are mainly concentrated in the range of $S_{1.4\text{GHz}} = 10 \sim 100$ mJy, but also as low as 2.6 ± 0.4 mJy. We find that the host galaxies of the associated HI absorbers have relatively high star formation rates, and there is a negative correlation between the HI column density and the stellar mass in the host galaxy. Consequently, FAST has significantly improved the capabilities and performance for HI absorption observations and has provided a true untargeted survey of 21 cm HI absorption galaxies for such studies.

Keywords: HI line emission (690), Extragalactic radio sources (508), Radio telescopes (1360), Redshift surveys (1378)

1. INTRODUCTION

Studies using the 21 cm HI emission line have played a key role in understanding the kinematics, structure, and evolution of galaxies in general (e.g., Giovanelli & Haynes 2015; Haynes et al. 2018; Zhang et al. 2024). However, the 21 cm HI absorption line is a more powerful tracer than the HI emission line on many scales, from the parsec scales near the central black hole to the tens of kpc structures tracing interactions and mergers of galaxies (Morganti & Oosterloo 2018). This is because the intensity of an HI absorption line depends on the intensity of the background continuum source, independent of redshift. Furthermore, HI absorption observations can be used to study the HI gas near an active nucleus out to much higher redshifts than is possible using HI emission, since the strong radio continuum emission is often associated with the central activity (e.g., Geréb et al. 2014, 2015; Darling et al. 2011; Curran et al. 2016; Curran & Duchesne 2018; Aditya & Kanekar 2018). Low redshift HI absorption line studies are also of great importance.

We can study these intriguing cases of spatially resolved HI absorption in low redshift HI absorbers. The 21 cm HI absorption surveys can also potentially identify primordial atomic gas, infalling or outflowing gas in the vicinity of galaxies or spiral disks. Therefore, HI absorption line observations are a good way to study the evolution of the HI properties of galaxies and related questions.

HI absorption observations have been made with all available radio telescopes, from single dish to interferometer (e.g., Dickey 1986; Gallimore et al. 1999; Mahony et al. 2013; Zwaan et al. 2015; Wu et al. 2015; Aditya & Kanekar 2018; Su et al. 2022; Hu et al. 2023; Yu et al. 2023; Aditya et al. 2024), but a number of limitations have affected HI absorption observations in the past (Morganti & Oosterloo 2018). One is the limited velocity range that can be covered by an observation while maintaining good spectral resolution. Another major limitation has been the limited coverage and sensitivity at lower frequencies, making it difficult to study high redshift objects. The third is the current lack of an untargeted survey of a very large volume of the Universe. Targeted observations focus primarily on extragalactic radio sources with sufficiently high fluxes. Consequently, they can only yield continuum-flux biased

HI absorber samples, underrepresenting galaxies with weak radio emission, but the weak radio sources can also give rise to noticeable absorption features (Sadler et al. 2007). Untargeted surveys could largely remove the effects of many of the selection biases that plague most studies today and sometimes make it difficult to draw firm conclusions. Darling et al. (2011) conducted an untargeted pilot survey for 21 cm HI absorption lines in a 517 deg^2 section of the ALFALFA survey at $z < 0.058$, but found no new absorption line systems. Hu et al. (2023) presented an untargeted search for the extragalactic 21 cm HI absorption lines with the Commensal Radio Astronomy FasT Survey (CRAFTS), but only two new and three known HI absorbers were detected. The First Large Absorption Survey in HI (FLASH; Alison et al. 2022) is a wide-field survey for HI absorption which is mainly covering the southern sky in the redshift range $0.42 < z < 1.00$ (e.g., Su et al. 2022; Aditya et al. 2024; Yoon et al. 2024). The MeerKAT Absorption Line Survey (MALS) was designed to perform an unbiased census of the HI and OH absorption lines at $0 < z < 2$ (Gupta et al. 2016). Therefore, further high-sensitivity, broadband, large-scale, and unbiased HI absorption surveys are important and needed to overcome the above difficulty.

The Five-hundred-meter Aperture Spherical radio Telescope (FAST) All Sky HI survey (FASHI) aims to cover the entire sky visible to FAST, between declinations of -14° and $+66^\circ$, within a frequency range of $1.0 - 1.5 \text{ GHz}$ (Nan et al. 2011; Jiang et al. 2019, 2020). The survey currently has a typical map rms of $\sim 0.76 \text{ mJy beam}^{-1}$ with a velocity resolution of 6.4 km s^{-1} for HI line (Zhang et al. 2024), while the Arecibo Legacy Fast ALFA Survey (ALFALFA) has a lower detection sensitivity of $\sim 1.86 \text{ mJy beam}^{-1}$ after smoothing to a velocity resolution of 10 km s^{-1} (Haynes et al. 2018). This suggests that the FASHI could detect more HI absorbers than the ALFALFA. Furthermore, the Ultra-Wide Bandwidth (UWB) receiver on FAST can simultaneously cover a frequency range of $500\text{-}3300 \text{ MHz}$, making FAST a powerful instrument for observing the high redshift HI absorbers in extragalactic objects (Zhang et al. 2023). Therefore, FAST with 19-beam and UWB receivers could be used to carry out such surveys mentioned above.

In this paper we mainly report an untargeted survey of 21 cm HI absorption galaxies with FAST over an area of about 10000 square degrees (see Figure 1). We discovered 51 HI absorbers, including 21 previously

known and 30 new ones at redshift $z \lesssim 0.09$ ¹. Currently, there are about 200 known HI absorbers in the literature (e.g., Morganti & Oosterloo 2018; Zhang et al. 2021; Su et al. 2022; Hu et al. 2023; Yu et al. 2023; Aditya et al. 2024). FAST has significantly improved the capabilities and performance for HI absorption observations compared to previous observations. Section 2 shows the FAST observations, data reduction, and source identification. Section 3 presents the characterization of the detected HI absorbers and lists their parameters. Section 4 discusses the properties of the detected HI absorbers and the host galaxies. Section 5 is a summary and talks about future work. Throughout this paper, we assume a Λ CDM cosmology with $H_0 = 75 \text{ km s}^{-1} \text{ Mpc}^{-1}$, $\Omega_M = 0.3$, and $\Omega_\Lambda = 0.7$.

2. OBSERVATIONS AND DATA PROCESSING

2.1. Observations

The 21 cm HI absorption spectral data come from the FASHI project (Zhang et al. 2024). The FAST 19-beam receiver was employed to efficiently cover the FAST sky. The aperture of FAST is 500 m, while the effective aperture is approximately 300 m, resulting in a beam size of $\sim 2.9'$ at 1.4 GHz. The full band of 500 MHz in the spectral line backend has a frequency coverage of 1000 to 1500 MHz with a total of 64k channels. The corresponding frequency resolution is 7.63 kHz or 1.6 km s^{-1} at 1.4 GHz for the raw data. The pointing error is less than or equal to $15''$. To calibrate intensity, a high-noise signal with an amplitude of $\sim 11 \text{ K}$ was injected into the entire FASHI observation for a period of 32 or 64 seconds. The factor of degrees per flux unit (DPFU) is relevant for 19 beams, with a value of $\text{DPFU} = 13 \sim 17 \text{ K Jy}^{-1}$ at a frequency of 1400 MHz, as detailed in Nan et al. (2011); Jiang et al. (2019, 2020). The FASHI project is predominantly performed using the drift scan mode. Throughout the survey, the telescope's azimuth arm was positioned on the meridian at a pre-assigned J2000 declination, with a spacing of $21'.65$ between primary drift centers. The feed array was rotated by 23.4° to enable super-Nyquist sampling of Earth-rotation drift-scan tracks of individual beams in the declination of J2000 coordinates, with sampling rates smaller than half the FWHM.

2.2. Data reduction

Currently, we only use the datasets in the frequency range of above 1305.5 MHz (or $z \lesssim 0.09$) due to serious RFI and relatively low sensitivity at low frequency

¹ The HI absorbers with $z \gtrsim 0.09$ will be released soon in the next work.

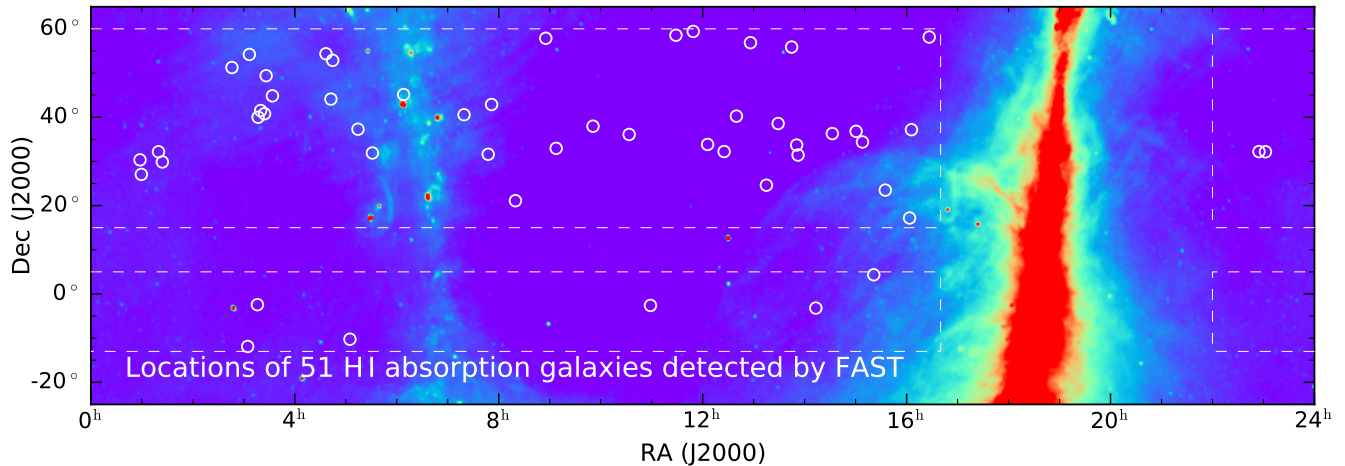


Figure 1. Locations for 51 HI absorption galaxies detected by FASHI over an area of about 10000 square degrees. The circles indicate their positions in the equatorial coordinate system. The background image is the all-sky 21-cm radio continuum of Stockert 25 m (Reich 1982) and Villa Elisa 30 m (Reich & Reich 1986; Reich et al. 2001). The white dashed rectangles indicate roughly the area currently covered by FAST.

ranges (see Zhang et al. 2022). The FASHI data are reduced using the FAST spectral data reduction pipeline, HiFAST (Jing et al. 2024). The HiFAST pipeline combines data reduction packages, including antenna temperature correction, baseline correction, RFI mitigation, standing wave correction, gridding, flux correction, and fits cube generation. In baseline correction, we utilized the Asymmetrically Reweighted Penalized Least Squares algorithm (arPLS; Baek et al. 2015) to adjust the spectral baseline. Several frequency periods (~ 1 MHz, ~ 2 MHz, and ~ 0.04 MHz) of standing waves are inhabited in the FASHI spectral data. The spectral quality can be significantly improved if the standing wave is completely corrected. Standing waves are predominantly fitted and subtracted using the SW package in the HiFAST pipeline (Jing et al. 2024). The data have been smoothed to a spectral resolution of $\sim 6.4 \text{ km s}^{-1}$ per channel and the fits cubes have been gridded to a pixel scale of 1 arcmin. A heliocentric velocity correction has been applied to the data due to the Doppler effect. A more detailed observation setup and data reduction procedure is presented in the FASHI paper by Zhang et al. (2024).

2.3. Source finding

The process of extracting sources for FASHI is comprised of two steps, involving both automated and interactive procedures. The application utilized for identifying sources within HI data cubes is designated as the HI Source Finding Application (SoFiA) in version 2². The SoFiA source finding algorithm involves the smoothing

of the data on various spatial and spectral scales specified by the user, along with the measurement of the noise level in each smoothing iteration. Subsequently, a user-defined flux threshold is applied relative to the noise in order to retain all pixels with statistically significant flux density. The fully automated and reliable source finding tool, SoFiA, is crucial for the scientific success of surveys (e.g., Westmeier et al. 2022; Zhang et al. 2024).

In the SoFiA setup, the detection threshold is 4.5σ (σ means the local noise level within the bounding box of the source in native units of the data cube; see the SoFiA Cookbook); the smoothing kernels are `kernelsXY = 0, 3, 6` and `kernelsZ = 0, 3, 7, 15` respectively; in the linking parameters, the minimum size of the sources in the spatial dimension is 5 pixels/channels each in XY and Z space, while the maximum size is 50 pixels in XY space, but not limited in Z space; furthermore, we set the `reliability.enable` to false, so that artifacts such as RFI and bad baselines occasionally remain in the spectral data. Based on the above setup, we found that the source candidates found by SoFiA contain some false signals. Therefore, a manual interactive source extraction has to be done, judging by the source moment maps, spectral profile, signal-to-noise ratio, and so on.

The HI absorption source finding procedure is similar to the HI emission source extraction in FASHI (Zhang et al. 2024). The only difference is to let `input.invert` be true, so that to search for negative signals, such as absorption lines.

The candidates found by SoFiA include fake sources due to RFI in FAST observation (e.g., Zhang et al. 2022). A manual source extraction is needed to judge

² <https://github.com/SoFiA-Admin/SoFiA-2>

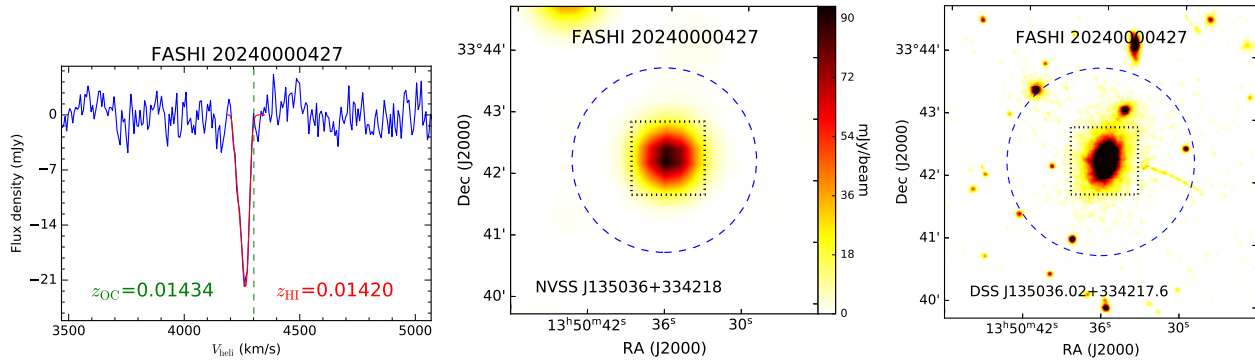


Figure 2. HI absorption galaxy FASHI 135036.30+334216.5 or ID 20240000427. *Left:* HI absorption spectrum. The HI redshift measured by FAST (in red) and an optical spectroscopic redshift (in green) are presented in the panel. The red curve line is the fit to the spectrum, and the green dashed line is the optical spectroscopic redshift. *Middle:* Blue circle indicates the position of HI source with a beam size of $\sim 2.9'$. The background shows 1.4 GHz radio continuum distribution. The bright source within a square is the radio counterpart. *Right:* The background shows DSS image. The bright source within a square is the DSS counterpart. The other 50 HI absorption galaxies are shown in the online version of Figure 2.

the source moment maps, spectral profile, signal to noise ratio, coordinate, flux density, optical counterparts and radio continuum sources, and then discard fake sources.

As for FASHI ID 20240000003, 20240000024, and 20240000022, the flux densities of the absorption peaks are not below zero, although they exhibit clear absorption characteristics. They thus cannot be extracted using the aforementioned method. In fact, the three sources were extracted from the FASHI emission sources by manual checking (Zhang et al. 2024).

In the end, we discovered and confirmed 51 HI absorber, including 21 previously known and 30 new ones (see Figures 1 and 2). Detailed information on these sources is presented in Appendix A.

2.4. Line fitting

Gaussian fitting has been widely employed to derive absorption line properties, such as the width of the profile, and to ascertain the presence of multiple components (e.g., Zhang et al. 2021; Hu et al. 2023). When multiple peaked profiles occur, as is the case in our absorption sample, Gaussian fitting methods have the disadvantage of necessitating a prior assumption regarding the physical conditions of the gas, namely the number of components to be fitted. The busy-function fitting method, as described in Westmeier et al. (2014), was employed in this study. This method has been successfully utilized in Geréb et al. (2015).

In the context of line fitting, if there is only one absorption line present, it is possible to utilise the busy-function fitting method to fit the absorption line directly. In the case that an emission line exists, but the absorption line is not obscured by a nearby emission line, the emission line will be masked first, and then the absorption line will be fitted (e.g., FASHI 20240000196,

20240000264, 20240000051, 20240000013). In the case that the absorption line is inaccessible to the emission line, the absorption line is masked, and then the emission line is fitted. Subsequently, the original line is employed to subtract the emission, after which the absorption line can be fitted (e.g., FASHI 20240000005, 20240000472, 20240000016).

3. DETECTION RESULTS AND ANALYSIS

3.1. Locations of FASHI HI absorbers

The FASHI data has already covered over an area of about 10000 square degrees within $0^h \lesssim \text{RA} \lesssim 24^h$, $-14^\circ \lesssim \text{Dec} \lesssim 66^\circ$ with a typical spectral detection sensitivity of ~ 1.50 mJy for a velocity resolution of ~ 6.4 km s $^{-1}$ at 1.4 GHz. Because the FASHI project can only operate in schedule-filler mode, parts of the above sky areas are not fully covered. In Figure 1 we show the locations of 51 HI absorption sources already detected by FAST at $z \lesssim 0.09$. This suggests that the current detection rate of the HI absorbers is 5.1×10^{-3} sources per square degree, while the FASHI HI emission sources have a detection rate of about 5.5 sources per square degree (Zhang et al. 2024). Based on this detection rate, we estimate that the probability of occurrence for the HI absorbers in all HI galaxies is $1/1078^3$. However, considering that the survey area does not have uniform sensitivity⁴, the measured detection rate is approximate. At the current detection sensitivity, the final number of HI absorbers detected by FASHI would

³ In this work, 51 HI absorbers are detected in an area of about 10000 square degrees. The probability of occurrence for the HI absorbers in all HI galaxies is $51/(5.5 \times 10000) \approx 1/1078$.

⁴ The sensitivity map is shown in Zhang et al. (2024)

be about 100 if FAST were able to cover 22000 square degrees at $z \lesssim 0.09$.

The ALFALFA survey used the seven-beam Arecibo *L*-band Feed Array to perform a drift-scan survey, covering an area of about 7000 square degrees over a redshift range of $z < 0.06$ and cataloging 31502 HI emission galaxies. Wu et al. (2015) predicted that the whole ALFALFA could eventually produce about 25 HI absorbers. Their probability of occurrence is about 1/1260 in all HI galaxies. This number is slightly lower than that found by FASHI.

Additionally, from Figure 1 we can see that the sources are mostly located at $30^\circ \lesssim \text{Dec} \lesssim 60^\circ$. This is because the current FASHI observations focus mainly on $30^\circ \lesssim \text{Dec} \lesssim 60^\circ$, where the data rms is much better than the region of $-15^\circ \lesssim \text{Dec} \lesssim 30^\circ$. In the near future FASHI will spend more time observing the region of $-15^\circ \lesssim \text{Dec} \lesssim 30^\circ$ and it is expected that the number of detections over that area will increase. With increasing detection sensitivity and area, the FASHI HI absorber sample could be expected to be much larger than the current number.

3.2. Coordinate catalog

Table 1 presents the source coordinates and counterparts of FASHI HI absorption galaxies. Each column is introduced as follows:

- Column 1: Index number for each FASHI HI source. This index number is unique to each FASHI source.
- Column 2: Centroid coordinate (J2000) for each FASHI HI source in the format of `Jhhmmss.ss±ddmmss.s`.
- Columns 3-4: Right ascension (RA) and declination (Dec) in units of deg from the FASHI source centroid (J2000).
- Column 5: Centroid coordinate (J2000) or name for each NVSS radio source in the format of `Jhhmmss±ddmmss` (Condon et al. 1998).
- Column 6: Centroid coordinate (J2000) for each optical counterpart in the format of `Jhhmmss.ss±ddmmss.s`.
- Column 7: Representatives of the corresponding galaxy counterparts.

3.3. Physical parameter catalog

Table 2 presents the physical parameters of FASHI HI absorption galaxies. Each column is introduced as follows:

- Column 1: Index number for each FASHI HI source. This index number is unique to each FASHI source.
- Column 2: Heliocentric velocity of the HI source in units of km s^{-1} . All results are presented in this work using the optical heliocentric definition of velocity.
- Column 3: Redshift, z_{HI} of the 21 cm HI line, corresponding to the heliocentric velocity in Column 2.
- Column 4: Redshift, z_{OC} of the optical counterparts collected from the literature.
- Column 5: Velocity width of the HI absorption line profile, W_{50} in km s^{-1} , measured at the level of 50% of the peak using the busy-function fitting method (Westmeier et al. 2014).
- Column 6: The depth of the HI absorption line, S_{HI} in mJy in negative value.
- Column 7: Integrated 1.4 GHz continuum flux density of radio source, $S_{1.4\text{GHz}}$ in mJy as provided by NVSS survey (Condon et al. 1998).
- Column 8: Assuming isotropic emission for a source, the radio luminosity (power) is calculated with the following relation (Yun et al. 2001):

$$\log \frac{L_{1.4\text{GHz}}}{\text{W Hz}^{-1}} = 17.08 + 2 \log \frac{D_L}{\text{Mpc}} + \log \frac{S_{1.4\text{GHz}}}{\text{mJy}}, \quad (1)$$

where D_L is the cosmological luminosity distance in Mpc and was calculated with a calculator from Wright (2006).

- Column 9: Optical depth τ_{HI} , estimated with equation (e.g., Wolfe & Burbidge 1975):

$$\tau_{\text{HI}} \approx -\ln\left(1 + \frac{S_{\text{HI}}}{c_f S_{1.4\text{GHz}}}\right), \quad (2)$$

where we assume covering factor $c_f = 1$ (Morganti & Oosterloo 2018) indicating the fraction of background radio continuum intercepted by the foreground HI cloud, S_{HI} and $S_{1.4\text{GHz}}$ are listed in the above columns.

- Column 10: HI column density, N_{HI} can be estimated with equation (e.g., Wolfe & Burbidge 1975):

$$N_{\text{HI}} = 1.823 \times 10^{18} T_s \int \tau_{\text{HI}} dV, \quad (3)$$

where we assume spin temperature $T_s = 100$ K for the HI gas (Morganti & Oosterloo 2018).

Table 1. Coordinates and counterparts of FASHI HI absorption galaxies

[1] FASHI ID	[2] FASHI J2000	[3] RA deg	[4] Dec deg	[5] NVSS J2000	[6] OC J2000	[7] Galaxy
20240000480	J030428.71-115315.1	46.1196	-11.8875	J030429-115422	J030429.63-115422.4	IRAS03021-1205
20240000482	J050451.78-101501.7	76.2157	-10.2505	J050453-101451	J050453.06-101452.5	IRAS05025-1018
20240000405	J141310.09-031140.8	213.2921	-3.1947	J141314-031227	J141314.84-031227.2	NGC5506
20240000476	J105833.00-023559.1	164.6375	-2.5997	J105835-023552	J105835.37-023551.9	PGC156086
20240000399	J031558.84-022532.1	48.9952	-2.4256	J031600-022539	J031600.78-022538.2	NGC1266
20240000093	J152121.51+042039.1	230.3396	4.3442	J152122+042033	J152122.54+042030.1	PGC054794
20240000483	J160329.87+171133.9	240.8745	17.1927	J160332+171158	J160332.09+171155.3	NGC6034
20240000003	J081937.14+210636.1	124.9048	21.1100	J081937+210653	J081937.95+210651.6	UGC04332
20240000408	J153455.59+233013.2	233.7316	23.5037	J153457+233011	J153457.38+233012.0	IC1127 IC4553 Arp220
20240000409	J131501.12+243651.4	198.7546	24.6143	J131503+243707	J131503.52+243707.7	IC0860
20240000116	J005922.61+270337.1	14.8442	27.0603	J005924+270332	J005924.43+270332.3	IC0064 UGC00613
20240000122	J012406.73+295238.5	21.0281	29.8774	J012407+295246	J012407.50+295244.0	LEDA1881594
20240060788	J005747.27+302108.9	14.4469	30.3525	J005748+302114	J005748.89+302108.8	NGC0315
20240000140	J135215.88+312631.6	208.0662	31.4421	J135217+312646	J135217.82+312646.6	UGC08782 3C293
20240000155	J074735.82+313625.2	116.8992	31.6070	J074742+313757	J074736.14+313659.6	PGC1955807
20240000014	J053117.26+315418.4	82.8219	31.9051	J053118+315412	J053118.79+315412.3	NVSSJ053118+315412
20240000159	J011932.90+321101.9	19.8871	32.1839	J011935+321050	J011935.00+321050.1	4C31.04
20240000027	J230222.13+321111.5	345.5922	32.1865	J230221+321125	J230222.47+321120.6	PGC070309
20240000026	J225442.56+321324.2	343.6773	32.2234	J225445+321248	J225444.97+321249.2	PGC069981
20240000129	J122512.74+321353.4	186.3031	32.2315	J122513+321401	J122513.11+321401.6	PGC1987158
20240000141	J090733.90+325729.4	136.8912	32.9582	J090734+325722	J090734.87+325723.1	PGC165523
20240000427	J135036.30+334216.5	207.6513	33.7046	J135036+334218	J135036.02+334217.6	NGC5318
20240000196	J120547.43+335016.9	181.4476	33.8380	J120547+335024	J120547.67+335022.1	PGC083530
20240000174	J150803.69+342339.2	227.0154	34.3942	J150805+342323	J150805.08+342315.9	PGC054033 IRAS15060+3434
20240000243	J103327.36+360550.9	158.3640	36.0975	J103328+360606	J103328.56+360559.5	PGC2074966
20240000024	J143235.35+361806.7	218.1473	36.3019	J143239+361808	J143239.90+361808.2	NGC5675
20240000037	J150033.79+364829.3	225.1408	36.8081	J150034+364844	J150034.58+364845.0	2MASXJ150034+364845
20240000039	J160542.81+371049.2	241.4284	37.1803	J160543+371046	J160543.21+371044.7	PGC084723
20240000036	J051419.90+371721.2	78.5829	37.2892	J051421+371714	J051421.10+371714.0	NVSSJ051421+371714
20240000500	J095055.65+375800.8	147.7319	37.9669	J095058+375758	J095058.71+375758.7	PGC090952
20240000022	J132849.73+383419.9	202.2072	38.5722	J132852+383438	J132852.11+383439.5	UGC08471
20240000443	J031646.12+395955.4	49.1921	39.9987	J031646+400011	J031646.70+400013.0	UGC02625 IC311
20240000264	J123943.52+401459.7	189.9313	40.2499	J123945+401450	J123945.16+401448.9	PGC089547
20240000051	J071908.19+403355.0	109.7841	40.5653	J071908+403343	J071908.66+403341.5	LAMOSTJ071908.70+403341.7
20240000445	J032421.15+404714.8	51.0881	40.7874	J032422+404719	J032422.86+404719.2	IRAS03211+4036 UGC2715
20240000501	J031946.81+413034.4	49.9450	41.5096	J031948+413042	J031948.26+413041.4	3C84 NGC1275
20240000013	J075134.30+425242.1	117.8929	42.8784	J075135+425249	J075135.64+425248.3	UGC04056
20240000454	J044226.82+440615.0	70.6117	44.1042	J044228+440638	J044228.49+440638.5	NVSSJ044228+440638
20240000059	J033337.92+445011.9	53.4080	44.8366	J033337+444941	J033337.90+444949.0	NVSSJ033337+444941
20240000507	J060801.90+450814.2	92.0079	45.1373	J060803+450825	J060803.44+450825.0	LEDA5061018
20240000078	J032614.32+492357.3	51.5597	49.3993	J032615+492357	J032616.00+492359.0	NVSSJ032615+492357
20240000512	J024600.14+511458.1	41.5006	51.2495	J024600+511515	J024600.54+511514.0	IRAS02425+5102
20240000007	J044433.30+525213.5	71.1388	52.8704	J044434+525224	J044434.76+525224.8	2MASXJ04443470+5252243
20240000083	J030630.87+541208.7	46.6286	54.2024	J030632+541158	J030632.74+541158.5	NVSSJ030632+541158
20240000005	J043636.25+542201.5	69.1510	54.3671	J043638+542159	J043638.61+542159.3	2MASXJ04363857+5421598
20240000023	J134440.84+555306.2	206.1702	55.8850	J134442+555313	J134442.09+555312.8	UGC08696 Mrk273
20240000513	J125614.58+565222.9	194.0608	56.8730	J125614+565223	J125614.17+565225.1	UGC08058 Mrk231
20240000515	J085519.79+575155.5	133.8324	57.8654	J085521+575143	J085519.04+575140.7	SDSSJ085519.04+575140.7
20240000472	J162636.67+580849.8	246.6528	58.1472	J162637+580911	J162637.74+580904.3	SDSSJ162637.74+580904.2
20240000016	J112832.57+583323.0	172.1357	58.5564	J112832+583346	J112831.99+583346.8	NGC3690
20240000471	J114852.43+592501.9	177.2185	59.4172	J114850+592457	J114850.36+592456.4	NGC3894

Notes. The FASHI IDs in bold indicate newly discovered absorber.

Table 2. Physical parameters of FASHI HI absorption galaxies

[1]	[2]	[3]	[4]	[5]	[6]	[7]	[8]	[9]	[10]
FASHI ID	V_{heli} km s^{-1}	z_{HI}	z_{OC}	W_{50} km s^{-1}	S_{HI} mJy	$S_{1.4\text{GHz}}$ mJy	$\log L_{1.4\text{GHz}}$ W Hz^{-1}	τ_{HI}	N_{HI} 10^{21}cm^{-2}
20240000480	6960.0	0.02322	0.03077	48.7 ± 4.8	-19.03 ± 2.56	29.4 ± 1.3	22.75	1.042 ± 0.260	9.26 ± 2.31
20240000482	11837.5	0.03949	0.04032	176.2 ± 7.8	-34.20 ± 1.19	1482.4 ± 44.5	24.69	0.023 ± 0.001	0.75 ± 0.03
20240000405	1809.4	0.00604	0.00607	72.3 ± 5.8	-32.97 ± 1.96	338.8 ± 10.2	22.38	0.102 ± 0.007	1.35 ± 0.09
20240000476	10888.2	0.03632	0.03622	115.9 ± 9.0	-16.25 ± 1.33	205.4 ± 6.2	23.74	0.082 ± 0.007	1.74 ± 0.16
20240000399	2172.1	0.00725	0.00732	88.6 ± 8.3	-8.33 ± 0.60	115.6 ± 3.5	22.08	0.075 ± 0.006	1.21 ± 0.10
20240000093	15660.3	0.05224	0.05216	25.5 ± 3.6	-20.20 ± 1.88	407.3 ± 13.4	24.36	0.051 ± 0.005	0.24 ± 0.02
20240000483	10224.0	0.03410	0.03402	25.4 ± 4.3	-28.35 ± 2.21	456.0 ± 15.2	24.03	0.064 ± 0.006	0.30 ± 0.03
20240000003	5444.8	0.01816	0.01842	158.1 ± 9.6	-5.02 ± 0.34	32.9 ± 1.4	22.34	0.166 ± 0.014	4.77 ± 0.41
20240000408	5435.7	0.01813	0.01810	334.9 ± 4.2	-50.51 ± 0.66	326.3 ± 9.8	23.32	0.168 ± 0.006	10.27 ± 0.37
20240000409	3903.1	0.01302	0.01291	116.1 ± 10.6	-11.67 ± 0.76	30.8 ± 1.0	22.00	0.476 ± 0.045	10.08 ± 0.94
20240000116	13960.5	0.04657	0.04583	25.8 ± 1.8	-70.19 ± 3.33	112.6 ± 4.0	23.69	0.977 ± 0.098	4.59 ± 0.46
20240000122	16656.6	0.05556		129.0 ± 10.0	-11.05 ± 0.64	27.1 ± 0.9	23.24	0.524 ± 0.046	12.32 ± 1.09
20240060788	5412.4	0.01805	0.01746	10.2 ± 1.6	-114.01 ± 24.82	772.1 ± 25.3	23.67	0.160 ± 0.038	0.30 ± 0.07
20240000140	13445.5	0.04485	0.04519	57.8 ± 2.1	-257.61 ± 4.20	4085.4 ± 144.0	25.23	0.065 ± 0.003	0.69 ± 0.03
20240000155	17767.5	0.05927	0.06055	381.4 ± 10.9	-6.61 ± 0.27	7.3 ± 0.5	22.75	2.352 ± 0.761	163.56 ± 52.93
20240000014	19953.8	0.06656	0.06120	87.0 ± 4.1	-22.58 ± 1.38	39.8 ± 1.3	23.50	0.838 ± 0.091	13.29 ± 1.44
20240000159	18153.2	0.06055	0.05996	12.9 ± 1.8	-68.26 ± 4.13	2635.2 ± 79.1	25.30	0.026 ± 0.002	0.06 ± 0.00
20240000027	6411.2	0.02139	0.02128	145.2 ± 17.6	-6.78 ± 1.63	2.6 ± 0.4	21.37	2.303 ± 1.000	60.94 ± 26.47
20240000026	6252.9	0.02086	0.02169	58.0 ± 9.1	-9.56 ± 0.98	32.0 ± 1.0	22.48	0.355 ± 0.046	3.75 ± 0.48
20240000129	17951.4	0.05988	0.05923	61.3 ± 8.7	-5.50 ± 0.47	49.3 ± 1.5	23.56	0.118 ± 0.011	1.32 ± 0.13
20240000141	14732.8	0.04914	0.04906	78.3 ± 4.6	-23.02 ± 0.92	46.8 ± 1.5	23.37	0.677 ± 0.050	9.67 ± 0.71
20240000427	4256.6	0.01420	0.01434	48.6 ± 4.8	-21.78 ± 1.16	101.1 ± 3.1	22.61	0.243 ± 0.017	2.15 ± 0.15
20240000196	15762.2	0.05258	0.05388	86.6 ± 12.6	-5.21 ± 0.49	8.5 ± 0.5	22.71	0.949 ± 0.175	14.98 ± 2.77
20240000174	13484.4	0.04498	0.04503	117.7 ± 3.2	-52.47 ± 1.24	133.1 ± 4.0	23.74	0.501 ± 0.025	10.76 ± 0.53
20240000243	17503.2	0.05838	0.05876	18.8 ± 2.7	-13.73 ± 1.88	105.4 ± 3.2	23.88	0.140 ± 0.021	0.48 ± 0.07
20240000024	3947.6	0.01317	0.01325	15.9 ± 0.0	-9.90 ± 0.00	118.8 ± 3.6	22.61	0.087 ± 0.003	0.25 ± 0.01
20240000037	19850.7	0.06621	0.06605	61.6 ± 3.9	-16.20 ± 2.01	57.3 ± 1.8	23.72	0.332 ± 0.051	3.74 ± 0.57
20240000039	19906.3	0.06640	0.06649	39.6 ± 0.0	-8.68 ± 1.47	28.4 ± 1.2	23.42	0.365 ± 0.077	2.64 ± 0.56
20240000036	22626.6	0.07547		19.2 ± 2.2	-17.23 ± 1.80	143.3 ± 4.3	24.24	0.128 ± 0.015	0.45 ± 0.05
20240000500	12199.6	0.04069	0.04053	31.8 ± 1.8	-50.84 ± 1.99	66.4 ± 2.0	23.35	1.451 ± 0.161	8.41 ± 0.94
20240000022	7837.8	0.02614	0.02649	25.7 ± 6.0	-11.34 ± 1.74	11.1 ± 1.3	22.19	2.303 ± 1.000	10.78 ± 4.68
20240000443	4276.0	0.01426	0.01419	25.4 ± 4.4	-11.05 ± 1.73	35.2 ± 1.4	22.14	0.377 ± 0.074	1.74 ± 0.34
20240000264	15751.0	0.05254	0.05386	294.1 ± 0.0	-1.32 ± 0.09	15.2 ± 0.6	22.96	0.091 ± 0.007	4.87 ± 0.40
20240000051	19848.0	0.06621	0.06593	101.6 ± 3.7	-8.03 ± 0.61	16.9 ± 0.6	23.19	0.645 ± 0.076	11.95 ± 1.40
20240000445	3842.8	0.01282	0.01299	37.3 ± 8.3	-12.28 ± 1.66	55.5 ± 1.7	22.26	0.250 ± 0.039	1.70 ± 0.27
20240000501	8115.0	0.02707	0.01754	10.9 ± 2.4	-2196.30 ± 10.16	22829.2 ± 684.9	25.14	0.101 ± 0.003	0.20 ± 0.01
20240000013	9223.3	0.03077	0.03203	127.9 ± 17.1	-5.27 ± 0.53	2.7 ± 0.4	21.75	2.303 ± 1.000	53.67 ± 23.31
20240000454	5362.5	0.01789		179.3 ± 8.7	-23.78 ± 0.92	54.9 ± 1.7	22.54	0.568 ± 0.038	18.56 ± 1.24
20240000059	19841.4	0.06618		26.6 ± 6.7	-6.61 ± 1.29	10.3 ± 0.5	22.98	1.027 ± 0.359	4.98 ± 1.74
20240000507	10214.9	0.03407	0.03566	36.6 ± 2.3	-25.54 ± 1.11	56.2 ± 1.7	23.16	0.606 ± 0.044	4.04 ± 0.29
20240000078	23584.3	0.07867		167.3 ± 2.7	-31.48 ± 2.20	64.0 ± 2.0	23.93	0.677 ± 0.074	20.64 ± 2.26
20240000512	10463.7	0.03490	0.03476	73.9 ± 1.5	-157.22 ± 2.33	223.5 ± 6.7	23.74	1.216 ± 0.079	16.37 ± 1.07
20240000007	9943.1	0.03317	0.03273	95.5 ± 6.5	-12.66 ± 1.09	77.2 ± 2.4	23.22	0.179 ± 0.018	3.12 ± 0.31
20240000083	19527.9	0.06514		35.8 ± 4.1	-9.26 ± 0.80	55.3 ± 1.7	23.70	0.183 ± 0.018	1.19 ± 0.12
20240000005	5647.5	0.01884		37.9 ± 3.1	-10.56 ± 1.20	58.7 ± 1.8	22.61	0.198 ± 0.026	1.37 ± 0.18
20240000023	11288.1	0.03765	0.03732	521.8 ± 11.9	-12.57 ± 0.58	144.7 ± 5.1	23.61	0.091 ± 0.006	8.64 ± 0.52
20240000513	12650.1	0.04220	0.04176	188.0 ± 11.5	-16.77 ± 0.73	308.9 ± 12.1	24.04	0.056 ± 0.003	1.91 ± 0.11
20240000515	7737.9	0.02581	0.02601	10.4 ± 0.0	-101.22 ± 11.53	651.6 ± 19.6	23.94	0.169 ± 0.022	0.32 ± 0.04
20240000472	4836.8	0.01613		26.0 ± 2.5	-60.37 ± 3.88	532.9 ± 18.3	23.44	0.120 ± 0.009	0.57 ± 0.04
20240000016	3140.3	0.01047	0.01044	214.6 ± 1.4	-69.90 ± 0.78	677.1 ± 25.4	23.16	0.109 ± 0.005	4.26 ± 0.18
20240000471	3292.4	0.01098	0.01081	158.0 ± 8.5	-24.73 ± 1.19	481.4 ± 14.4	23.04	0.053 ± 0.003	1.52 ± 0.09

Notes. The FASHI IDs in bold are first discovered in this work. For FASHI 20240000013, 20240000022, and 20240000027, $|S_{\text{HI}}|$ is larger than $S_{1.4\text{GHz}}$, we assume $S_{\text{HI}}/S_{1.4\text{GHz}} = -0.9$ for τ_{HI} estimation. Perhaps the line intensity measurements have a large uncertainty due to the mixing between the emission and absorption lines. Further confirmation, such as high spatial resolution observations, is needed to explain this.

Table 3. Cross-matched sources between the absorbers and GSWLC.

[1]	[2]	[3]	[4]	[5]	[6]	[7]	[8]	[9]	[10]	[11]
FASHI ID	OBJID	RA	Dec	z_{\odot}	$\log(M_{\star})$	$\log(\text{SFR}_{\text{SED}})$	A_V	g	r	z
B1950		deg	deg		M_{\odot}	$M_{\odot} \text{ yr}^{-1}$	mag	mag	mag	mag
20240000093	1237662266464600297	230.344	4.342	0.0522	11.55 ± 0.00	-0.52 ± 0.14	0.15 ± 0.03	14.65	13.72	13.01
20240000483	1237665440998031492	240.884	17.199	0.0340	11.20 ± 0.01	0.33 ± 0.05	0.49 ± 0.01	13.95	13.08	12.40
20240000003	1237664836462182621	124.908	21.114	0.0185	10.82 ± 0.04	0.65 ± 0.03	0.76 ± 0.01	14.27	13.44	12.76
20240000408	1237665537075511390	233.738	23.504	0.0184	10.87 ± 0.02	0.37 ± 0.08	0.69 ± 0.07	13.59	12.93	12.40
20240000140	1237665331471515679	208.075	31.446	0.0452	11.33 ± 0.01	0.85 ± 0.07	0.68 ± 0.08	14.62	13.74	13.04
20240000155	1237657595683406347	116.910	31.633	0.0600	9.54 ± 0.07	-0.09 ± 0.08	0.16 ± 0.05	16.16	15.50	15.01
20240000129	1237665329852842117	186.305	32.234	0.0592	11.59 ± 0.01	0.17 ± 0.27	0.43 ± 0.10	14.85	13.97	13.26
20240000141	1237660763766849674	136.895	32.956	0.0491	11.05 ± 0.03	0.67 ± 0.11	0.63 ± 0.08	15.47	14.61	14.21
20240000427	1237665025986986033	207.650	33.705	0.0143	10.90 ± 0.01	-0.42 ± 0.23	0.49 ± 0.03	13.04	12.17	11.89
20240000174	1237662306730967257	227.039	34.422	0.0453	9.19 ± 0.08	-0.38 ± 0.08	0.17 ± 0.05	16.35	15.55	16.00
20240000243	1237662224058220698	158.369	36.100	0.0588	11.17 ± 0.01	0.33 ± 0.12	0.12 ± 0.04	15.76	14.96	14.42
20240000024	1237662305117143073	218.166	36.302	0.0132	10.98 ± 0.02	-0.18 ± 0.31	0.56 ± 0.10	13.02	12.22	11.77
20240000037	1237661850409304180	225.144	36.813	0.0661	10.97 ± 0.01	-0.27 ± 0.26	0.23 ± 0.07			
20240000039	1237662303518457905	241.430	37.179	0.0665	10.58 ± 0.08	0.91 ± 0.12	0.39 ± 0.12	16.42	15.78	15.41
20240000022	1237664294759366699	202.234	38.574	0.0265	10.15 ± 0.04	-0.08 ± 0.48	0.50 ± 0.10	14.24	13.47	13.03
20240000023	1237661387602853939	206.176	55.887	0.0373	10.77 ± 0.05	0.35 ± 0.33	0.39 ± 0.14	14.74	14.00	13.62
20240000515	1237651274037329931	133.829	57.861	0.0260	9.15 ± 0.05	-0.78 ± 0.04	0.13 ± 0.00	17.34	16.77	16.78
20240000016	1237655107301277787	172.140	58.563	0.0105	10.40 ± 0.04	0.85 ± 0.08	0.86 ± 0.09	12.47	11.90	11.98
20240000471	1237655107839393797	177.267	59.433	0.0107	10.45 ± 0.03	-0.32 ± 0.26	0.46 ± 0.09	12.11	11.29	10.97

Notes. In this catalog, the listed Columns [2]-[8] are taken from GSWLC (Salim et al. 2016) and the Columns [9]-[11] are taken from the SGA catalog.

3.4. Absorbers cross-matching with GSWLC

Table 3 shows the 19 sources recovered when the FASHI observed absorbers are cross-matched with the GALEX-SDSS-WISE Legacy Catalog (GSWLC) catalog (Salim et al. 2016) under the condition $\delta_{\text{RA}} \leq 3'$, $\delta_{\text{Dec}} \leq 3'$ and $\delta_{\text{HI velocity}} \leq 300 \text{ km s}^{-1}$. Furthermore, the cross-matched sources could be classified as associated absorption, since the redshift difference between the HI absorption and the background is much smaller than 3000 km s^{-1} (e.g., Aditya et al. 2024). Each column in Table 3 is introduced as follows:

- Column 1: Index number for each FASHI HI source. This index number is unique to each FASHI source.
- Column 2: OBJID, SDSS photometric identification number, from GSWLC.
- Columns 3-4: RA and Dec with centroid coordinate (J2000) in units deg, from GSWLC.
- Column 5: Redshift, z_{\odot} , from GSWLC.
- Column 6: Stellar mass, $\log(M_{\star})$ with its error, from GSWLC.

- Column 7: UV/optical (SED) star formation rate, $\log(\text{SFR}_{\text{SED}})$ with its error, from GSWLC.
- Column 8: Dust attenuation, A_V , in rest-frame V , from GSWLC.
- Columns 9-11: g , r , and z band photometry, in AB mag, from the local galaxy sample Siena Galaxy Atlas (SGA).

4. DISCUSSION

4.1. Comparison with known detections

In Figure 3, two examples of FAST spectra are superimposed on Arecibo spectra (Mirabel & Sanders 1988; Springob et al. 2005). The both show good agreement in velocity and flux. We also checked other previously observed HI absorbers in Appendix A. We found that most of the absorbers have good agreement in flux, e.g., 20240000405, 20240000116, and 20240000014. In fact, we have made a detailed comparison between FASHI and ALFALFA survey data in Zhang et al. (2024). Comparisons of the measured rms, SNR, and integrated flux parameters between FASHI and ALFALFA sources suggest that FAST provides highly reliable data sets. How-

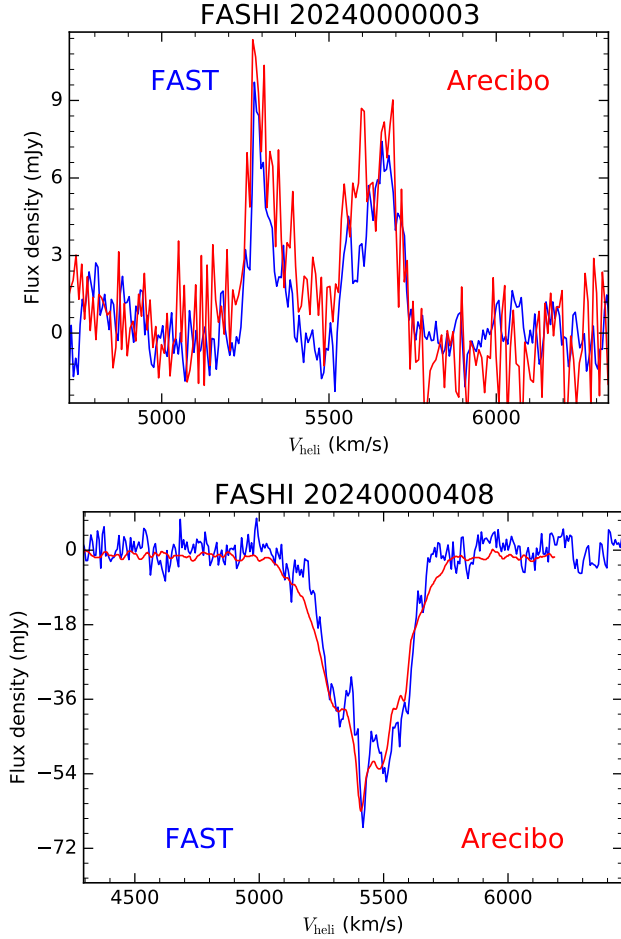


Figure 3. Two examples of FAST spectra superimposed on Arecibo spectra (Mirabel & Sanders 1988; Springob et al. 2005). The both show good agreement in velocity and flux.

ever, there are also some absorbers that have large flux discrepancies between FAST and the other instruments. A likely reason is that the low spatial resolution observations may introduce large flux pollution from nearby objects or unknown RFI, and the high spatial resolution VLBI observations may miss some flux due to lack of large scale structure coverage.

4.2. Luminosity across redshift

Figure 4 shows the luminosity-redshift distribution, which includes 51 HI absorbers observed by FASHI, some sample compiled by Geréb et al. (2015), Maccagni et al. (2017), and Curran & Duchesne (2018). A notable difference is that the measured 1.4 GHz continuum luminosity of the background sources towards the FASHI absorbers is lower than that for the sample in Geréb et al. (2015), Maccagni et al. (2017), and Curran & Duchesne (2018). Figure 4 shows that the radio flux densities of the FASHI absorbers are mainly concentrated in the flux

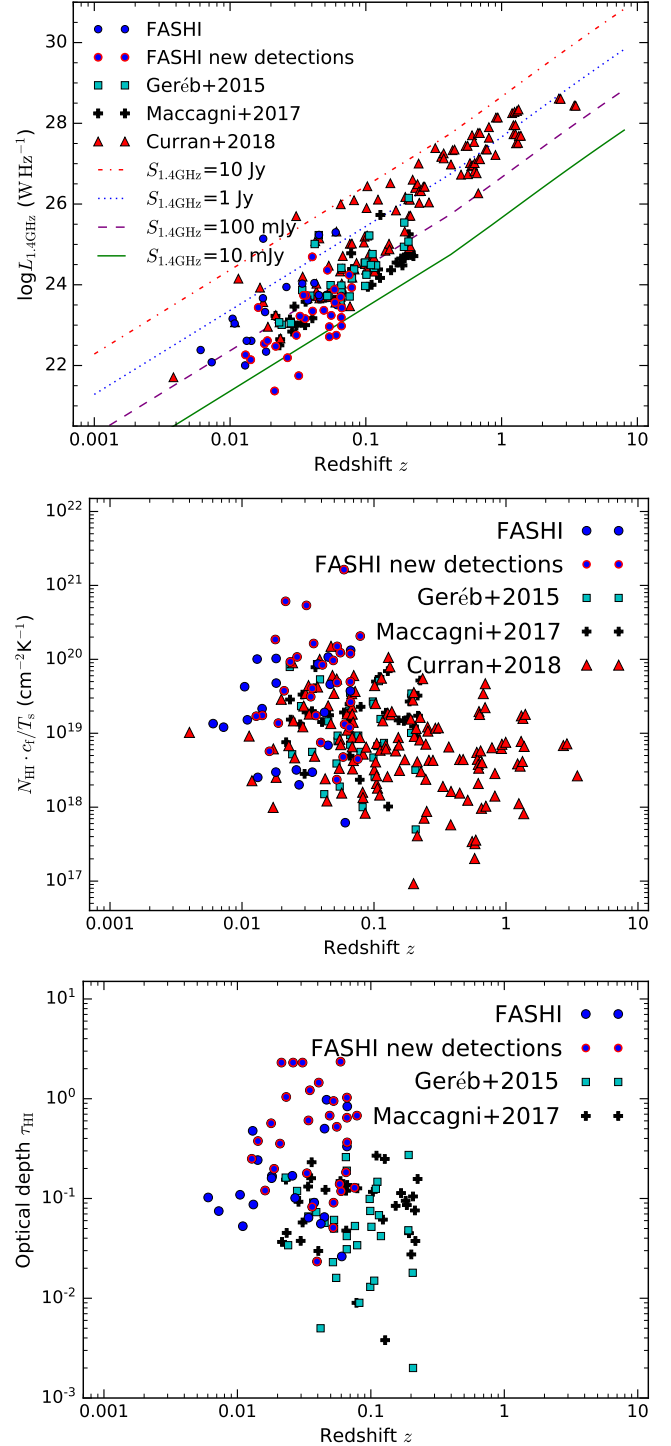


Figure 4. The rest-frame 1.4 GHz continuum luminosity (*upper*) of the background sources, the HI column density (*middle*), and the HI optical depth versus redshift (*lower*) for the 21-cm HI absorbers, including data points from Geréb et al. (2015), Maccagni et al. (2017), Curran & Duchesne (2018), and FASHI. In the upper panel, the different lines indicate different 1.4 GHz continuum flux density.

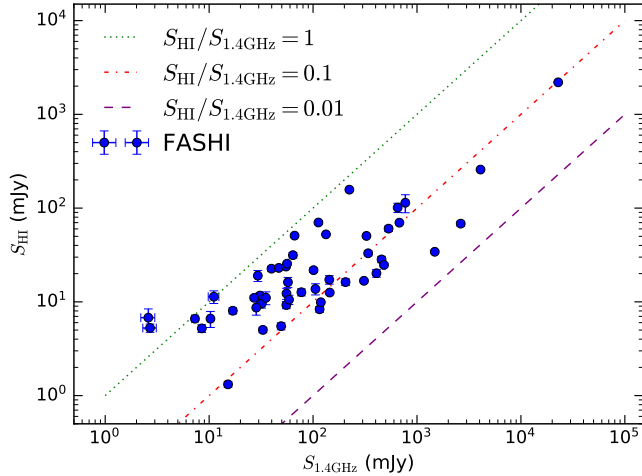


Figure 5. The distribution between the depth of the HI absorption line (S_{HI}) and the integrated 1.4 GHz continuum flux density ($S_{1.4\text{GHz}}$) for the detected absorbers by FASHI.

density range of $S_{1.4\text{GHz}} = 10 \sim 100$ mJy, but even as low as 2.6 ± 0.4 mJy for FASHI2024000027. The absorbers in the Geréb et al. (2015), Maccagni et al. (2017), and Curran & Duchesne (2018) sample are located at $S_{1.4\text{GHz}} = 100 \sim 10000$ mJy. The discrepancy is probably due to the selection effect. For example, the sample in Geréb et al. (2015), Maccagni et al. (2017), and Curran & Duchesne (2018) come from the flux-selected sources, whereas the FASHI absorbers represent a completely untargeted and unbiased survey.

Figure 5 shows the distribution between the depth of the HI absorption line (S_{HI}) and the integrated 1.4 GHz continuum flux density ($S_{1.4\text{GHz}}$) for the absorbers detected by FASHI. We find that many detected absorbers have a relatively lower 1.4 GHz continuum flux density ($S_{1.4\text{GHz}} = 10$ mJy) than previous flux-selected surveys, which usually have a selection threshold of $S_{1.4\text{GHz}} > 50$ mJy (e.g., Yun et al. 2001; Geréb et al. 2014, 2015; Curran & Duchesne 2018).

4.3. Column density and optical depth across redshift

Figure 4 also shows the distribution between the HI column density and redshift for the 51 HI absorbers detected by FASHI and some other sample compiled by Geréb et al. (2015), Maccagni et al. (2017), and Curran & Duchesne (2018). The column densities vary from 6.2×10^{19} to 1.6×10^{23} cm^{-2} , and the median is 3.7×10^{21} cm^{-2} for the FASHI data. It also shows that there is no apparent number variation across redshift, which is consistent with the previous result measured by Gupta et al. (2006). However, we found weak evidence of a dependence on redshift among all data points, including FASHI, Geréb et al. (2015), Maccagni

et al. (2017), and Curran & Duchesne (2018). Figure 4 also shows the distribution between HI optical depth and redshift for the 51 HI absorbers detected by FASHI and some other samples compiled by Geréb et al. (2015) and Maccagni et al. (2017). It also shows that there is no apparent number variation across redshift. We also found weak evidence for a redshift dependence among all data points, including FASHI, Geréb et al. (2015) and Maccagni et al. (2017). The negative correlation in column density and optical depth across redshift may be due to different detection limits.

4.4. Distribution of velocity

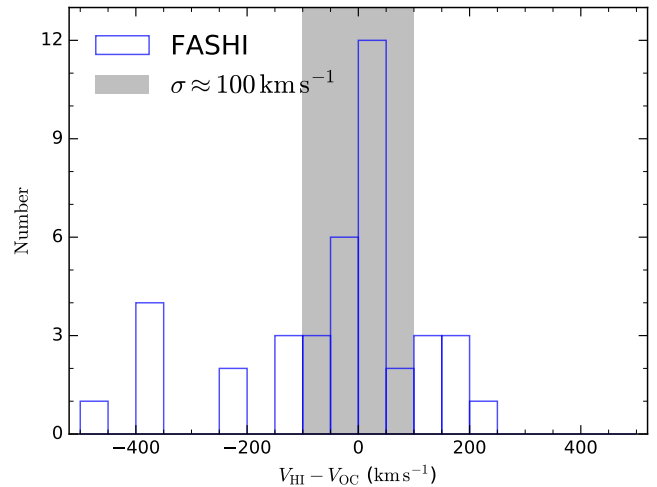


Figure 6. The histogram of velocities for the principal HI absorption components with respect to the systemic velocity estimated from optical counterparts. The derived velocity error is about $\sigma = 100$ km s^{-1} shown with a shaded bar.

The morphology and kinematics of HI gas in radio galaxies are found to be very complex. HI can trace rotating disks, offset clouds, and complex morphological structures of unsettled gas, such as infall and outflow (Geréb et al. 2015). HI gas associated with the circumnuclear disk/torus and rotating around the nucleus may appear both blue- and redshifted relative to the systemic velocity (Chandola et al. 2013). Figure 6 shows the velocity distribution for the main HI absorption components with respect to the systemic velocity estimated from the optical counterparts. We have a total of 43 samples in this figure, since other samples have no known spectroscopic redshift parameters. We find that the number of blue-shifted and redshifted absorbers is 20 and 23, respectively. It seems that in this untargeted survey the redshifted number is slightly higher than the blueshifted number. However, if we consider the uncertainties of the systemic velocity ($\sigma \approx 100$ km s^{-1}), the

number of blue- and redshifted absorbers should be almost equal (see Figure 6). We also found that there are four blueshifted absorbers at $< -300 \text{ km s}^{-1}$, but none at the high redshifted position ($> 300 \text{ km s}^{-1}$). Therefore, blueshifted absorption is relatively more common, which is consistent with the previous conclusion in, e.g., Vermeulen et al. (2003). The relative velocity of the absorbing gas could be significantly blueshifted if it is due to gas which has been accelerated by interaction with the radio jet, while infalling material fuelling the central engine would appear redshifted. More recent studies (e.g., Geréb et al. 2015; Maccagni et al. 2017) also show that if the line profiles show HI gas deviating from regular rotation, this HI gas is mostly seen as blueshifted absorption. It is possible that the blueshifted absorption could be from AGN-driven outflows or driven by a radio jet. In addition, a very narrow and high redshifted absorption is detected and likely tracing an infalling cloud at larger distance from the nucleus.

4.5. Distributions of line width and optical depth

Figure 7 shows the distribution of line width for the 21 cm HI absorber measured by FASHI and Geréb et al. (2015). We find that 64.7% of the FASHI sample has a relatively narrow line width with $W_{50} < 100 \text{ km s}^{-1}$, while only 9.8% of the FASHI sample has a wide line width with $W_{50} > 200 \text{ km s}^{-1}$. FASHI 20240000023 has the widest line width with $W_{50} = 521.8 \pm 11.9 \text{ km s}^{-1}$. The sample in Geréb et al. (2015) has a similar trend in the distribution of the line width as the FASHI. Taylor et al. (1999) utilized VLBI to demonstrate that the narrow component could be observed against both jets and the nucleus, while the broad component is visible exclusively against the nucleus. They proposed that the broad component represents a circumnuclear torus, while the narrow component is indicative of inward-flowing cold gas. Beswick et al. (2004) also found that the narrow HI absorption lines are often attributed to gas at a distance from the center of the galaxy, as they are often indicative of absorption by ambient gas. Furthermore, major merger systems typically exhibit broad HI absorption profiles, which trace perturbed disk-like structures (e.g., Geréb et al. 2015; Maccagni et al. 2017).

Figure 7 shows the optical depth distribution for the 21 cm HI absorbers measured by FASHI and Geréb et al. (2015). In the FASHI sample, we find that most HI absorbers are optically thin with $N_{\tau_{\text{HI}} < 0.2} = 51.0\%$ and $N_{\tau_{\text{HI}} < 1.0} = 84.3\%$, and the median is $\tau_{\text{HI}} = 0.2$. We note that our measured optical depths are mostly higher than previous measurements (e.g., Geréb et al. 2015). This may be because our untargeted survey is not biased towards the strong radio continuum sources.

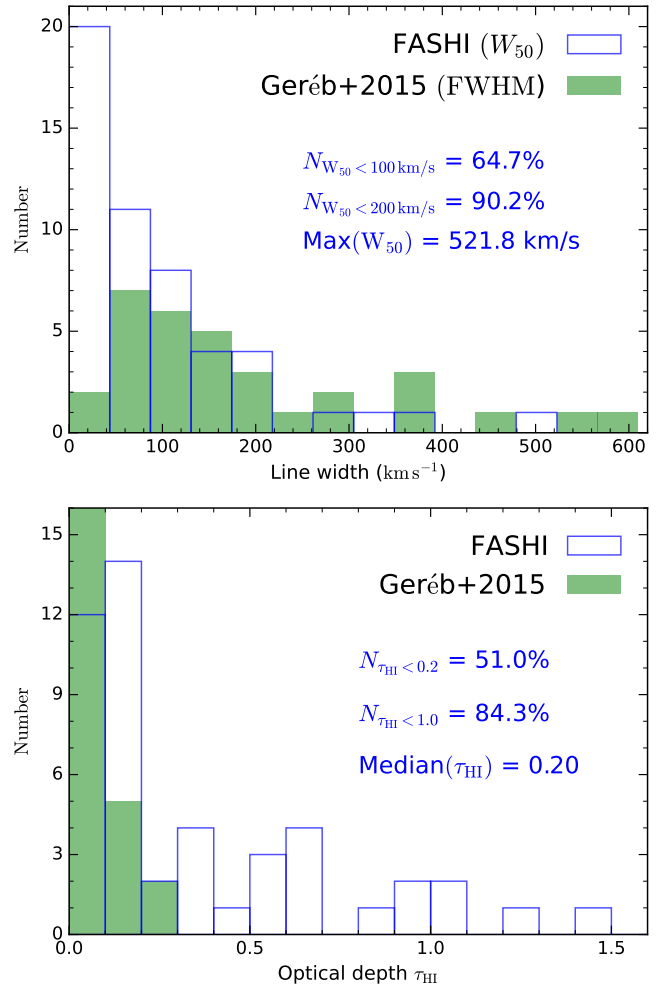


Figure 7. The histograms of line width (*upper*) and optical depth (*lower*) for the 21 cm HI absorbers in FASHI and Geréb et al. (2015).

4.6. Several special HI absorbers

Geréb et al. (2015) presented an analysis of the HI absorption in 32 objects observed with the Westerbork Synthesis Radio Telescope (WSRT). The 32 HI absorption sample show a broad variety of widths, shapes, and kinematical properties, but they do not include a kind of special line profile mentioned below. A common feature of such absorbers is the coexistence of an absorption line with an associated emission line. In the case of FASHI 20240000003, 20240000024, 20240000022, 20240000443, 20240000005, 20240000472, and 20240000016, the absorption line is situated in close proximity to the line centre of the emission line. In the case of FASHI 20240000196, 20240000264, and 20240000013, the absorption line is situated at the blueshifted wing of the emission profile. For FASHI 20240000027 and 20240000051, the absorption line is located at the red-

shifted wing of the emission line. The emission component may come from the nearby interacting galaxy or from the same galaxy as the absorbers. The coexistence of absorption and emission lines is very rare and requires high spatial resolution observations, such as VLBI, to resolve the host galaxy in order to understand their formation.

4.7. Host galaxy properties

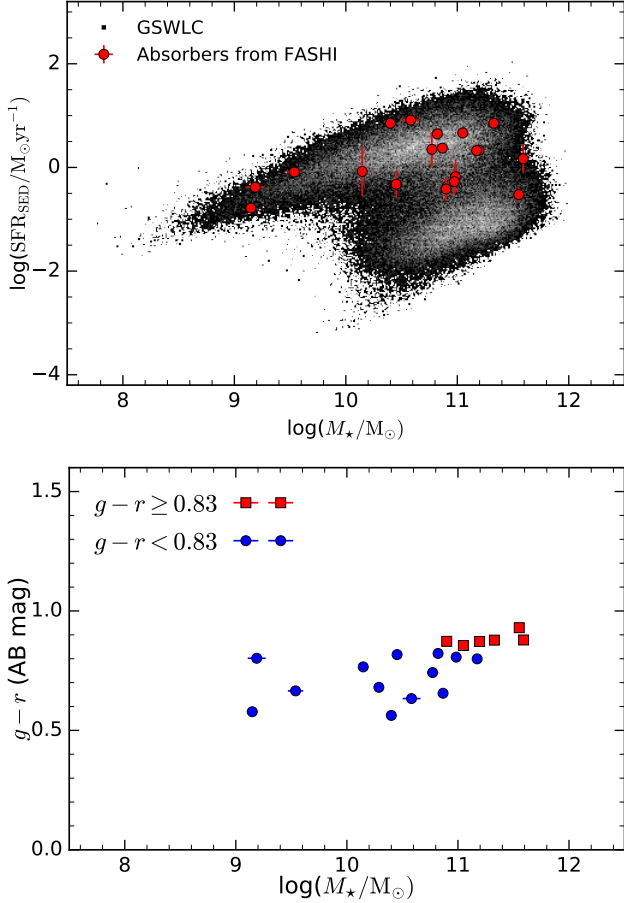


Figure 8. *Upper:* Two-dimensional distributions of star formation rate $\log(\text{SFR}_{\text{SED}})$ and stellar mass $\log(M_{\star})$. The background shows all the data in the GSWLC. The red dots indicate cross-matched and associated HI absorbers detected by FASHI. *Lower:* Color-stellar mass diagram of the FASHI absorbers. The blue and red galaxies are separated by $g-r = 0.83$ (Yang et al. 2006; Weinmann et al. 2006).

The cross-matched 19 absorbers in the upper panel of Figure 8 and Table 3 belong to the associated HI absorption and are also thought to originate from within the AGN host galaxy. The multi-wavelength SED fitting results in Figure 8 show that the associated HI absorbers host galaxies have relatively high star formation rates with $-0.78 \pm 0.04 < \log(\text{SFR}_{\text{SED}}) < 0.91 \pm 0.12 M_{\odot} \text{yr}^{-1}$,

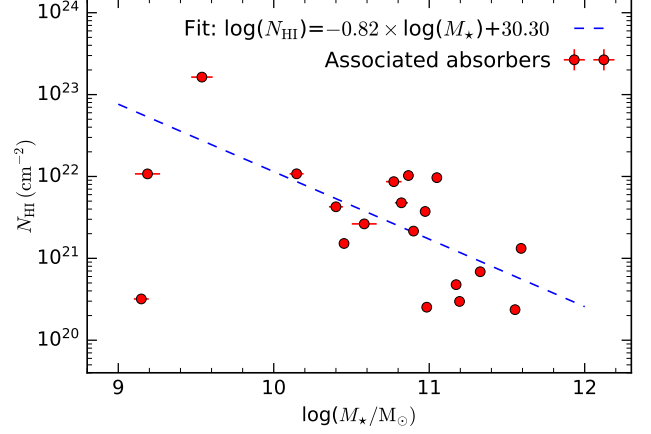


Figure 9. The relationship between the HI column density and the stellar mass in the host galaxy. The red dots indicate cross-matched and associated HI absorbers detected by FASHI.

and the stellar masses are in the range of $9.15 \pm 0.05 < \log(M_{\star}) < 11.59 \pm 0.01 M_{\odot}$.

The lower panel of Figure 8 shows the color-stellar mass diagram of the FASHI absorbers. The color magnitudes are taken from the SGA catalog. The blue and red galaxies are separated by $g-r = 0.83$ (Yang et al. 2006; Weinmann et al. 2006). We find that most of the sources are blue galaxies, and the red galaxies have colors close to the threshold of $g-r = 0.83$. This proves that the HI absorbers are more common in star-forming galaxies and less common in elliptical galaxies. This result is consistent with the inferred high star formation rates for the HI absorbers in the upper panel of Figure 8.

In Figure 9, we also plot the distribution between the HI column density and stellar mass $\log(M_{\star})$ for the cross-matched and associated HI absorbers detected by FAST. It presents a negative correlation between the HI column density and $\log(M_{\star})$. We then fit a relationship that is $\log(N_{\text{HI}}) = -0.82 \times \log(M_{\star}) + 30.30$. This may indicate that when the HI column density for the HI absorbers is high, the host galaxy has a low stellar mass. It is likely that the high-stellar-mass galaxies are in their old stage for HI absorbers, so gas in the AGN envelope is scarce. We also check the relationship between HI line width, star formation rates, and HI column density. However, we do not get a clear linear relationship.

4.8. Completeness and Reliability

In the current reduced FASHI data, the sensitivities for detection are uneven in different regions (see details in Zhang et al. 2024). This is because FASHI could only use the schedule-filler time. As a result, the completeness becomes relatively low at the regions with a

low detection sensitivity or a relatively high redshift. In addition, the strange gaps of the FASHI targets at ~ 190 , ~ 210 , and ~ 266 Mpc (see details in Zhang et al. 2024) also result in a relatively low completeness. A full test for completeness will be done with the HI emission sources and presented in a forthcoming paper, since the HI absorption sources have a much smaller sample for statistics.

The currently released HI absorbers were extracted using SoFiA with a threshold of 4.5σ . The sources were checked for reliability by interactive manual source extraction based on 0th, 1st and 2nd moments, integrated spectral profile and SNR ($\text{SNR} > 5.0$). Human intervention was used to optimize measurement accuracy and improve sample reliability by rejecting spurious detections corresponding to low-level RFI, poorly sampled data, and residual baseline fluctuations. The optical and radio counterparts of each source were identified and listed in Table 1. Out of 51 HI absorbers, only 8 sources have no corresponding spectroscopic redshift data, but they have obvious HI absorption line profiles and corresponding NVSS counterparts. As a result, all of the HI absorbers that have been released are of relatively high confidence.

5. SUMMARY AND FUTURE WORK

FASHI is designed to cover the entire sky observable by the Five-hundred-meter Aperture Spherical radio Telescope (FAST). Based on the FASHI data, in the first HI absorption data release we perform an untargeted survey of 21 cm HI absorption galaxies at redshift $z \lesssim 0.09$ over an area of about 10000 square degrees. With SoFiA source finding algorithm, we extracted 51 HI absorbers, including 21 previously known and 30 new ones, with 8 sources having no optical spectroscopic redshift. The current detection rate of the HI absorbers is 5.1×10^{-3} sources per square degree, while the FASHI HI emission sources have a detection rate of about 5.5 sources per square degree. We can further estimate that the probability of occurrence for the HI absorbers in all HI galaxies is 1/1078. With the current detection sensitivity, the final number of HI absorbers detected by FASHI would be about 100 if FAST were able to cover 22000 square degrees at $z \lesssim 0.09$. In the near future, the redshift will be extended to $z \gtrsim 0.09$, and many more absorbers would be detected and released.

The radio flux densities of the FASHI absorbers are mainly concentrated in the range of $S_{1.4\text{GHz}} = 10 \sim 100$ mJy, but also as low as 2.6 ± 0.4 mJy. We also find that 64.7% of the sample has a relatively narrow line width with $W_{50} < 100 \text{ km s}^{-1}$, while only 9.8% of the sample has a wide line width with $W_{50} > 200 \text{ km s}^{-1}$.

FASHI20240000023 has the widest line width with $W_{50} = 521.8 \pm 11.9 \text{ km s}^{-1}$. Such results would provide some important clues for future flux-selected HI absorber surveys. We also detected some special HI absorbers. A common feature is the coexistence of an absorption line with an associated emission line, for example FASHI 20240000003, 20240000024, 20240000022, 20240000443, 20240000005, 20240000472, 20240000016, 20240000196, 20240000264, 20240000013, 20240000027 and 20240000051. The emission component may originate from the nearby interacting galaxy or the same galaxy as the absorbers. High spatial resolution observations, such as VLBI, are necessary to conduct such studies.

We present the multi-wavelength SED fitting results for the associated HI absorption. We find that the host galaxies of the associated HI absorbers have relatively high star formation rates with $-0.78 \pm 0.04 < \log(\text{SFR}_{\text{SED}}) < 0.91 \pm 0.12 M_{\odot} \text{ yr}^{-1}$. We find a negative correlation between the HI column density and $\log(M_{\star})$ with a fit of $\log(N_{\text{HI}}) = -0.82 \times \log(M_{\star}) + 30.30$. This may indicate that when the HI column density for the HI absorbers is high, the host galaxy has a small stellar mass. We check the relationship between HI line width, star formation rates, and HI column density, but we do not get a clear linear relationship.

FAST has significantly improved the capabilities and performance for HI absorption observations, providing a true untargeted survey of 21 cm HI absorption galaxies for such studies over an area of about 10000 square degrees. However, the currently released data cover only a low redshift range with $z \lesssim 0.09$. With the accumulation of FAST observational data, higher redshifts up to $z \approx 0.42$ and larger area up to 18000 square degrees would be covered in 4-5 years. In addition, FAST with UWB receiver could cover much higher redshifts up to $z \approx 1.84$ (Zhang et al. 2023). The detection sensitivity would also be greatly improved. This will lead to the detection of more HI absorbers. We also plan to observe each HI absorber with single point observing mode to obtain its high sensitivity and high velocity resolution spectra, which could help us to clearly see the hyperfine velocity profile.

ACKNOWLEDGEMENTS

This work is supported by the National Key R&D Program of China (No.2022YFA1602901), the West Light Foundation of the Chinese Academy of Sciences, the National Natural Science Foundation of China (Nos.11803044, 11933003, 12173045, 12373001, 12373011, and 11933011), the science research grants from the China Manned Space Project (No. CMS-CSST-

2021-A05), and the Guizhou Provincial Science and Technology Projects (QKHFQ[2023]003, QKHPTRC-ZDSYS[2023]003, QKHFQ[2024]001-1). This work is also sponsored by the Chinese Academy of Sciences (CAS), through a grant to the CAS South America Center for Astronomy (CASSACA). FAST is a Chinese national mega-science facility, operated by the National Astronomical Observatories of Chinese Academy of Sci-

ences (NAOC). We also wish to thank the anonymous referee for comments that improved the clarity of the paper.

This research has made use of the SIMBAD database, operated at CDS, Strasbourg, France. This research has made use of the NASA/IPAC Extragalactic Database (NED), which is funded by the National Aeronautics and Space Administration and operated by the California Institute of Technology.

REFERENCES

- Aditya, J. N. H. S., & Kanekar, N. 2018, *MNRAS*, 481, 1578, doi: [10.1093/mnras/sty2184](https://doi.org/10.1093/mnras/sty2184)
- Aditya, J. N. H. S., Yoon, H., Allison, J. R., et al. 2024, *MNRAS*, 527, 8511, doi: [10.1093/mnras/stad3722](https://doi.org/10.1093/mnras/stad3722)
- Alatalo, K., Blitz, L., Young, L. M., et al. 2011, *ApJ*, 735, 88, doi: [10.1088/0004-637X/735/2/88](https://doi.org/10.1088/0004-637X/735/2/88)
- Allison, J. R., Sadler, E. M., Amaral, A. D., et al. 2022, *PASA*, 39, e010, doi: [10.1017/pasa.2022.3](https://doi.org/10.1017/pasa.2022.3)
- Baan, W. A., & Haschick, A. 1990, *ApJ*, 364, 65, doi: [10.1086/169385](https://doi.org/10.1086/169385)
- Baan, W. A., & Haschick, A. D. 1981, *ApJL*, 243, L143, doi: [10.1086/183461](https://doi.org/10.1086/183461)
- Baan, W. A., Haschick, A. D., & Greenfield, P. E. 1978, *ApJL*, 222, L7, doi: [10.1086/182680](https://doi.org/10.1086/182680)
- Baan, W. A., Wood, P. A. D., & Haschick, A. D. 1982, *ApJL*, 260, L49, doi: [10.1086/183868](https://doi.org/10.1086/183868)
- Baek, S.-J., Park, A., Ahn, Y.-J., & Choo, J. 2015, *The Analyst*, 140 1, 250
- Beswick, R. J., Peck, A. B., Taylor, G. B., & Giovannini, G. 2004, *MNRAS*, 352, 49, doi: [10.1111/j.1365-2966.2004.07892.x](https://doi.org/10.1111/j.1365-2966.2004.07892.x)
- Bicay, M. D., & Giovanelli, R. 1986, *AJ*, 91, 732, doi: [10.1086/114054](https://doi.org/10.1086/114054)
- Chandola, Y., Gupta, N., & Saikia, D. J. 2013, *MNRAS*, 429, 2380, doi: [10.1093/mnras/sts499](https://doi.org/10.1093/mnras/sts499)
- Condon, J. J., Cotton, W. D., Greisen, E. W., et al. 1998, *AJ*, 115, 1693, doi: [10.1086/300337](https://doi.org/10.1086/300337)
- Conway, J. E. 1996, in *Extragalactic Radio Sources*, ed. R. D. Ekers, C. Fanti, & L. Padrielli, Vol. 175, 92
- Courtois, H. M., & Tully, R. B. 2015, *MNRAS*, 447, 1531, doi: [10.1093/mnras/stu2405](https://doi.org/10.1093/mnras/stu2405)
- Curran, S. J., & Duchesne, S. W. 2018, *MNRAS*, 476, 3580, doi: [10.1093/mnras/sty443](https://doi.org/10.1093/mnras/sty443)
- Curran, S. J., Reeves, S. N., Allison, J. R., & Sadler, E. M. 2016, *MNRAS*, 459, 4136, doi: [10.1093/mnras/stw943](https://doi.org/10.1093/mnras/stw943)
- Darling, J., Macdonald, E. P., Haynes, M. P., & Giovanelli, R. 2011, *ApJ*, 742, 60, doi: [10.1088/0004-637X/742/1/60](https://doi.org/10.1088/0004-637X/742/1/60)
- de Vaucouleurs, G., de Vaucouleurs, A., & Corwin, J. R. 1976, *Second reference catalogue of bright galaxies*, 1976, 0
- De Young, D. S., Roberts, M. S., & Saslaw, W. C. 1973, *ApJ*, 185, 809, doi: [10.1086/152456](https://doi.org/10.1086/152456)
- Dickey, J. M. 1986, *ApJ*, 300, 190, doi: [10.1086/163793](https://doi.org/10.1086/163793)
- . 1997, *AJ*, 113, 1939, doi: [10.1086/118408](https://doi.org/10.1086/118408)
- Ferruit, P., Adam, G., Binette, L., & Pécontal, E. 1997, *NewA*, 2, 345, doi: [10.1016/S1384-1076\(97\)00023-7](https://doi.org/10.1016/S1384-1076(97)00023-7)
- Gallimore, J. F., Baum, S. A., O’Dea, C. P., Pedlar, A., & Brinks, E. 1999, *ApJ*, 524, 684, doi: [10.1086/307853](https://doi.org/10.1086/307853)
- Geréb, K., Maccagni, F. M., Morganti, R., & Oosterloo, T. A. 2015, *A&A*, 575, A44, doi: [10.1051/0004-6361/201424655](https://doi.org/10.1051/0004-6361/201424655)
- Geréb, K., Morganti, R., & Oosterloo, T. A. 2014, *A&A*, 569, A35, doi: [10.1051/0004-6361/201423999](https://doi.org/10.1051/0004-6361/201423999)
- Giovanelli, R., & Haynes, M. P. 2015, *A&A Rv*, 24, 1, doi: [10.1007/s00159-015-0085-3](https://doi.org/10.1007/s00159-015-0085-3)
- Gupta, N., Salter, C. J., Saikia, D. J., Ghosh, T., & Jeyakumar, S. 2006, *MNRAS*, 373, 972, doi: [10.1111/j.1365-2966.2006.11064.x](https://doi.org/10.1111/j.1365-2966.2006.11064.x)
- Gupta, N., Srianand, R., Baan, W., et al. 2016, in *MeerKAT Science: On the Pathway to the SKA*, 14, doi: [10.22323/1.277.0014](https://doi.org/10.22323/1.277.0014)
- Haynes, M. P., Giovanelli, R., Martin, A. M., et al. 2011, *AJ*, 142, 170, doi: [10.1088/0004-6256/142/5/170](https://doi.org/10.1088/0004-6256/142/5/170)
- Haynes, M. P., Giovanelli, R., Kent, B. R., et al. 2018, *ApJ*, 861, 49, doi: [10.3847/1538-4357/aac956](https://doi.org/10.3847/1538-4357/aac956)
- Heckman, T. M., Balick, B., & Sullivan, W. T., I. 1978, *ApJ*, 224, 745, doi: [10.1086/156423](https://doi.org/10.1086/156423)
- Helou, G., Madore, B. F., Schmitz, M., et al. 1991, in *Astrophysics and Space Science Library*, Vol. 171, *Databases and On-line Data in Astronomy*, ed. M. A. Albrecht & D. Egret, 89–106, doi: [10.1007/978-94-011-3250-3_10](https://doi.org/10.1007/978-94-011-3250-3_10)
- Hu, W., Wang, Y., Li, Y., et al. 2023, *A&A*, 675, A40, doi: [10.1051/0004-6361/202245549](https://doi.org/10.1051/0004-6361/202245549)

- Iwasawa, K., Mazzarella, J. M., Surace, J. A., et al. 2011, *A&A*, 528, A137, doi: [10.1051/0004-6361/201015872](https://doi.org/10.1051/0004-6361/201015872)
- Jiang, P., Yue, Y., Gan, H., et al. 2019, *Science China Physics, Mechanics, and Astronomy*, 62, 959502, doi: [10.1007/s11433-018-9376-1](https://doi.org/10.1007/s11433-018-9376-1)
- Jiang, P., Tang, N.-Y., Hou, L.-G., et al. 2020, *Research in Astronomy and Astrophysics*, 20, 064, doi: [10.1088/1674-4527/20/5/64](https://doi.org/10.1088/1674-4527/20/5/64)
- Jing, Y., Wang, J., Xu, C., et al. 2024, *Science China Physics, Mechanics, and Astronomy*, 67, 259514, doi: [10.1007/s11433-023-2333-8](https://doi.org/10.1007/s11433-023-2333-8)
- Lavaux, G., & Hudson, M. J. 2011, *MNRAS*, 416, 2840, doi: [10.1111/j.1365-2966.2011.19233.x](https://doi.org/10.1111/j.1365-2966.2011.19233.x)
- Maccagni, F. M., Morganti, R., Oosterloo, T. A., Geréb, K., & Maddox, N. 2017, *A&A*, 604, A43, doi: [10.1051/0004-6361/201730563](https://doi.org/10.1051/0004-6361/201730563)
- Mahony, E. K., Morganti, R., Emonts, B. H. C., Oosterloo, T. A., & Tadhunter, C. 2013, *MNRAS*, 435, L58, doi: [10.1093/mnrasl/slt094](https://doi.org/10.1093/mnrasl/slt094)
- Mirabel, I. F. 1983, *ApJL*, 270, L35, doi: [10.1086/184065](https://doi.org/10.1086/184065)
- Mirabel, I. F., & Sanders, D. B. 1988, *ApJ*, 335, 104, doi: [10.1086/166909](https://doi.org/10.1086/166909)
- Morganti, R., & Oosterloo, T. 2018, *A&A Rv*, 26, 4, doi: [10.1007/s00159-018-0109-x](https://doi.org/10.1007/s00159-018-0109-x)
- Nagar, N. M., Oliva, E., Marconi, A., & Maiolino, R. 2002, *A&A*, 391, L21, doi: [10.1051/0004-6361:20021039](https://doi.org/10.1051/0004-6361:20021039)
- Nan, R., Li, D., Jin, C., et al. 2011, *International Journal of Modern Physics D*, 20, 989, doi: [10.1142/S0218271811019335](https://doi.org/10.1142/S0218271811019335)
- Nilson, P. 1973, *Uppsala general catalogue of galaxies*
- Peck, A., & Taylor, G. B. 2000, in *EVN Symposium 2000, Proceedings of the 5th european VLBI Network Symposium*, ed. J. E. Conway, A. G. Polatidis, R. S. Booth, & Y. M. Pihlström, 119, doi: [10.48550/arXiv.astro-ph/0009373](https://doi.org/10.48550/arXiv.astro-ph/0009373)
- Reich, P., & Reich, W. 1986, *A&AS*, 63, 205
- Reich, P., Testori, J. C., & Reich, W. 2001, *A&A*, 376, 861, doi: [10.1051/0004-6361:20011000](https://doi.org/10.1051/0004-6361:20011000)
- Reich, W. 1982, *A&AS*, 48, 219
- Sadler, E. M., Cannon, R. D., Mauch, T., et al. 2007, *MNRAS*, 381, 211, doi: [10.1111/j.1365-2966.2007.12231.x](https://doi.org/10.1111/j.1365-2966.2007.12231.x)
- Salim, S., Lee, J. C., Janowiecki, S., et al. 2016, *ApJS*, 227, 2, doi: [10.3847/0067-0049/227/1/2](https://doi.org/10.3847/0067-0049/227/1/2)
- Springob, C. M., Haynes, M. P., Giovanelli, R., & Kent, B. R. 2005, *ApJS*, 160, 149, doi: [10.1086/431550](https://doi.org/10.1086/431550)
- Struve, C., & Conway, J. E. 2012, *A&A*, 546, A22, doi: [10.1051/0004-6361/201218768](https://doi.org/10.1051/0004-6361/201218768)
- Su, R., Sadler, E. M., Allison, J. R., et al. 2022, *MNRAS*, 516, 2947, doi: [10.1093/mnras/stac2257](https://doi.org/10.1093/mnras/stac2257)
- Taylor, G. B., O'Dea, C. P., Peck, A. B., & Koekemoer, A. M. 1999, *ApJL*, 512, L27, doi: [10.1086/311873](https://doi.org/10.1086/311873)
- Toba, Y., Oyabu, S., Matsuhara, H., et al. 2014, *ApJ*, 788, 45, doi: [10.1088/0004-637X/788/1/45](https://doi.org/10.1088/0004-637X/788/1/45)
- van Gorkom, J. H., Knapp, G. R., Ekers, R. D., et al. 1989, *AJ*, 97, 708, doi: [10.1086/115016](https://doi.org/10.1086/115016)
- Vermeulen, R. C., Pihlström, Y. M., Tschager, W., et al. 2003, *A&A*, 404, 861, doi: [10.1051/0004-6361:20030468](https://doi.org/10.1051/0004-6361:20030468)
- Wang, L.-L., Luo, A. L., Shen, S.-Y., et al. 2018, *MNRAS*, 474, 1873, doi: [10.1093/mnras/stx2798](https://doi.org/10.1093/mnras/stx2798)
- Weinmann, S. M., van den Bosch, F. C., Yang, X., & Mo, H. J. 2006, *MNRAS*, 366, 2, doi: [10.1111/j.1365-2966.2005.09865.x](https://doi.org/10.1111/j.1365-2966.2005.09865.x)
- Wenger, M., Ochsenein, F., Egret, D., et al. 2000, *A&AS*, 143, 9, doi: [10.1051/aas:2000332](https://doi.org/10.1051/aas:2000332)
- Westmeier, T., Jurek, R., Obreschkow, D., Koribalski, B. S., & Staveley-Smith, L. 2014, *MNRAS*, 438, 1176, doi: [10.1093/mnras/stt2266](https://doi.org/10.1093/mnras/stt2266)
- Westmeier, T., Deg, N., Spekkens, K., et al. 2022, *PASA*, 39, e058, doi: [10.1017/pasa.2022.50](https://doi.org/10.1017/pasa.2022.50)
- Wolfe, A. M., & Burbidge, G. R. 1975, *ApJ*, 200, 548, doi: [10.1086/153821](https://doi.org/10.1086/153821)
- Wright, E. L. 2006, *PASP*, 118, 1711, doi: [10.1086/510102](https://doi.org/10.1086/510102)
- Wu, Z. Z., Haynes, M. P., Giovanelli, R., Zhu, M., & Chen, R. R. 2015, *Acta Astronomica Sinica*, 56, 112
- Yang, X., van den Bosch, F. C., Mo, H. J., et al. 2006, *MNRAS*, 369, 1293, doi: [10.1111/j.1365-2966.2006.10373.x](https://doi.org/10.1111/j.1365-2966.2006.10373.x)
- Yoon, H., Sadler, E. M., Mahony, E. K., et al. 2024, *arXiv e-prints*, arXiv:2408.06626, doi: [10.48550/arXiv.2408.06626](https://doi.org/10.48550/arXiv.2408.06626)
- Yu, N., Ho, L. C., Wang, J., & Li, H. 2022, *ApJS*, 261, 21, doi: [10.3847/1538-4365/ac626b](https://doi.org/10.3847/1538-4365/ac626b)
- Yu, Q., Fang, T., Wang, J., & Wu, J. 2023, *ApJ*, 952, 144, doi: [10.3847/1538-4357/acdb76](https://doi.org/10.3847/1538-4357/acdb76)
- Yun, M. S., Reddy, N. A., & Condon, J. J. 2001, *ApJ*, 554, 803, doi: [10.1086/323145](https://doi.org/10.1086/323145)
- Zhang, B., Zhu, M., Wu, Z.-Z., et al. 2021, *MNRAS*, 503, 5385, doi: [10.1093/mnras/stab754](https://doi.org/10.1093/mnras/stab754)
- Zhang, C.-P., Xu, J.-L., Wang, J., et al. 2022, *Research in Astronomy and Astrophysics*, 22, 025015, doi: [10.1088/1674-4527/ac3f2d](https://doi.org/10.1088/1674-4527/ac3f2d)
- Zhang, C.-P., Jiang, P., Zhu, M., et al. 2023, *Research in Astronomy and Astrophysics*, 23, 075016, doi: [10.1088/1674-4527/acd58e](https://doi.org/10.1088/1674-4527/acd58e)
- Zhang, C.-P., Zhu, M., Jiang, P., et al. 2024, *SCPMA*, 67, 219511, doi: [10.1007/s11433-023-2219-7](https://doi.org/10.1007/s11433-023-2219-7)
- Zwaan, M. A., Liske, J., Péroux, C., et al. 2015, *MNRAS*, 453, 1268, doi: [10.1093/mnras/stv1717](https://doi.org/10.1093/mnras/stv1717)

APPENDIX

A. NOTES ON INDIVIDUAL SOURCES

In this work, the optical spectroscopic redshift parameters are mostly obtained from the local galaxy sample Siena Galaxy Atlas⁵ (SGA). Some other sample information comes from the SIMBAD Astronomical Database (Wenger et al. 2000) and the NASA/IPAC Extragalactic Database (Helou et al. 1991).

FASHI J030428.71-115315.1 or (ID 20240000480): This HI absorber seems to have been first discovered by FASHI. The optical redshift ($z_{OC} = 0.03077$; Lavaux & Hudson 2011) is $\sim 2266 \text{ km s}^{-1}$ larger than the measured HI redshift ($z_{HI} = 0.02322$).

FASHI J050451.78-101501.7 or (ID 20240000482): This HI absorber seems to have been first detected by FASHI. The radio source is the Seyfert 2 galaxy, IRAS 05025-1018 (Simbad).

FASHI J141310.09-031140.8 or (ID 20240000405): This absorber was reported e.g. by Dickey (1986). There are two absorption lines, located at $V_{\text{heli}} \approx 1800 \text{ km s}^{-1}$ and $V_{\text{heli}} \approx 2000 \text{ km s}^{-1}$. The measured spectral profile is in good agreement with that in Gallimore et al. (1999). The radio source belongs to the Seyfert galaxy (Gallimore et al. 1999; Nagar et al. 2002).

FASHI J105833.00-023559.1 or (ID 20240000476): This HI absorber seems to have been first detected by FASHI. The source is a radio galaxy.

FASHI J031558.84-022532.1 or (ID 20240000399): This absorber was reported e.g. by Alatalo et al. (2011). The measured flux density agrees well with that of Alatalo et al. (2011). The radio source is a lenticular galaxy NGC 1266 in the constellation Eridanus. The galaxy hosts an obscured active galactic nucleus (Alatalo et al. 2011).

FASHI J152121.51+042039.1 or (ID 20240000093): This HI absorber seems to have been first detected by FASHI. The radio source belongs to the Seyfert 2 galaxy.

FASHI J160329.87+171133.9 or (ID 20240000483): This absorber was first detected in absorption by VLA observations (Dickey 1997). The radio source is hosted by an S0 optical galaxy in cluster A2151 of the Hercules Supercluster (Geréb et al. 2015).

FASHI J081937.14+210636.1 or (ID 20240000003): The HI observations were presented by Bica & Giovanelli (1986); Springob et al. (2005). The radio source belongs to the Seyfert 2 galaxy.

FASHI J153455.59+233013.2 or (ID 20240000408): This absorber has been widely detected, e.g. by Dickey (1986). The radio source is a well-known starburst galaxy, Arp 220 or IC 4553 (Baan et al. 1982).

FASHI J131501.12+243651.4 or (ID 20240000409): The HI observations were presented by Mirabel & Sanders (1988); Courtois & Tully (2015). The radio source belongs to a LINER-type Active Galaxy Nucleus.

FASHI J005922.61+270337.1 or (ID 20240000116): This absorber was first reported with FAST by Zhang et al. (2021), but also detected by Hu et al. (2023). Our measured flux density is in good agreement with that of Hu et al. (2023).

FASHI J012406.73+295238.5 or (ID 20240000122): This HI absorber appears to have been first discovered by FASHI. There is no optical spectroscopic redshift in the previous literature.

FASHI J005747.27+302108.9 or (ID 20240060788): The HI observations were presented by Haynes et al. (2011). The radio source belongs to a LINER-type active galactic nucleus.

FASHI J135215.88+312631.6 or (ID 20240000140): This absorber was reported with FAST by Hu et al. (2023). This object is the famous disk galaxy 3C 0293. The HI outflow driven by the radio jet was reported by Mahony et al. (2013). The extremely broad and multi-component HI absorption feature may be indicative of a rotating disk (e.g., Baan & Haschick 1981; Beswick et al. 2004).

FASHI J074735.82+313625.2 or (ID 20240000155): This HI absorber seems to have been first detected by FASHI. The radio source is weak with $S_{1.4\text{GHz}} = 7.3 \pm 0.5 \text{ mJy}$, while the HI linewidth is broad with $W_{50} = 381.4 \pm 10.9 \text{ km s}^{-1}$. There are three optical counterparts near the radio source.

FASHI J053117.26+315418.4 or (ID 20240000014): This absorber was first detected with FAST by Hu et al. (2023), whose measured flux density is in good agreement with our detection in this paper. Hu et al. (2023) suggested unsettled gas structures or gas accretion onto the supermassive black hole (SMBH).

⁵ <https://www.legacysurvey.org/sga/sga2020/>

FASHI J011932.90+321101.9 or (ID 20240000159): This absorber was reported by [van Gorkom et al. \(1989\)](#); [Conway \(1996\)](#); [Gupta et al. \(2006\)](#); [Struve & Conway \(2012\)](#); [Morganti & Oosterloo \(2018\)](#). It has two HI absorption velocity components. The low velocity is slightly blueshifted ($\sim 40 \text{ km s}^{-1}$), while the high velocity is redshifted ($\sim 200 \text{ km s}^{-1}$), relative to the systemic velocity of the galaxy. The low-velocity component may trace the rotating HI disk, and the high-velocity component may be due to small clouds evaporating from the inner edge of the disk ([Gupta et al. 2006](#)).

FASHI J230222.13+321111.5 or (ID 20240000027): The HI line was presented by [Courtois & Tully \(2015\)](#); [Yu et al. \(2022\)](#), but its HI absorption feature was first discovered by FASHI. The radio source belongs to the Low Surface Brightness Galaxy.

FASHI J225442.56+321324.2 or (ID 20240000026): This HI absorber seems to have been first detected by FASHI. The galaxy is in a group of galaxies. In the foreground is the Milky Way, which may interfere with detecting the optical counterpart.

FASHI J122512.74+321353.4 or (ID 20240000129): This HI absorber seems to have been first detected by FASHI. The radio source belongs to the Seyfert 2 galaxy.

FASHI J090733.90+325729.4 or (ID 20240000141): This HI absorber seems to have been first detected by FASHI. There is no further information about this object.

FASHI J135036.30+334216.5 or (ID 20240000427): This absorber was reported by [Mirabel \(1983\)](#). The radio source is a LINER-type active galactic nucleus. That the observed HI absorption occurs in clouds close to the nucleus ([Mirabel 1983](#)).

FASHI J120547.43+335016.9 or (ID 20240000196): This HI absorber seems to have been first discovered by FASHI. The HI line shows not only an absorption feature but also an emission line profile that agrees well with the redshift of the optical counterpart.

FASHI J150803.69+342339.2 or (ID 20240000174): This absorber was reported by [Baan et al. \(1978\)](#). The optical counterpart is a binary galaxy system that is connected to each other by a visible bridge (see Figure 2).

FASHI J103327.36+360550.9 or (ID 20240000243): This HI absorber appears to have been first discovered by FASHI. There is no further information on this object.

FASHI J143235.35+361806.7 or (ID 20240000024): The radio source is a known Seyfert 2 galaxy, NGC 5675. This source was observed by [Dickey \(1986\)](#), but they did not detect an HI absorption feature. With FAST we detected a faint and narrow absorption line at the center of the HI emission line.

FASHI J150033.79+364829.3 or (ID 20240000037): This absorber was reported by [Geréb et al. \(2015\)](#). The HI line is close to the systemic velocity of the host galaxy and may trace a regularly rotating HI disk ([Geréb et al. 2015](#)).

FASHI J160542.81+371049.2 or (ID 20240000039): This HI absorber seems to have been first detected by FASHI. The radio source is a LINER-type active galactic nucleus.

FASHI J051419.90+371721.2 or (ID 20240000036): This HI absorber seems to have been first detected by FASHI. There is no further information about this object. In the foreground is the Milky Way, which may interfere with detecting the optical counterpart.

FASHI J095055.65+375800.8 or (ID 20240000500): This HI absorber seems to have been first detected by FASHI. The radio source belongs to the Seyfert galaxy ([Toba et al. 2014](#)).

FASHI J132849.73+383419.9 or (ID 20240000022): This HI absorber seems to have been first discovered by FASHI. The HI line shows not only an absorption feature but also an emission line profile. The HI line shows a narrow absorption feature at the center of the broad emission line.

FASHI J031646.12+395955.4 or (ID 20240000443): This HI absorber seems to have been first detected by FASHI. The HI line shows not only an absorption feature but also an emission line profile. The HI line shows a prominent absorption feature that nearly coincides with the mean velocity of the emission signal. The HI line profile of this source is almost identical to that of NGC 984 reported by [Mirabel \(1983\)](#). NGC 984 has a compact bright core with an extended halo. It is a low surface brightness galaxy.

FASHI J123943.52+401459.7 or (ID 20240000264): This HI absorber seems to have been first detected by FASHI. The HI line shows not only an absorption feature but also an emission line profile. There is also an HI emission line that agrees well with the redshift of the optical counterpart.

FASHI J071908.19+403355.0 or (ID 20240000051): This HI absorber seems to have been first detected by FASHI. The HI line shows not only an absorption feature but also an emission line profile. There is also an HI emission line at a low velocity position. In the foreground is the Milky Way, which may interfere with detecting the optical counterpart. The radio source belongs to the Seyfert galaxy ([Wang et al. 2018](#)).

FASHI J032421.15+404714.8 or (ID 20240000445): This HI absorber seems to have been first discovered by FASHI. In the foreground is the Milky Way, which may interfere with detecting the optical counterpart.

FASHI J031946.81+413034.4 or (ID 20240000501): This absorber has been widely reported e.g. by De Young et al. (1973); Ferruit et al. (1997). The radio source is the well-known Seyfert 2 galaxy, 3C 84. The absorbing systems have two very different velocities. The high velocity system is a relatively narrow HI absorption line redshifted $\sim 3000 \text{ km s}^{-1}$ from the systemic velocity of 3C 84 (De Young et al. 1973).

FASHI J075134.30+425242.1 or (ID 20240000013): This HI absorber seems to have been first discovered by FASHI. The HI line shows not only an absorption feature but also an emission line profile. The HI absorption line is located at the blueshift wing of the double peak HI emission profile. The radio source belongs to a LINER-type active galactic nucleus.

FASHI J044226.82+440615.0 or (ID 20240000454): This HI absorber seems to have been first detected by FASHI. There is no further information about this object. In the foreground is the Milky Way, which may interfere with detecting the optical counterpart.

FASHI J033337.92+445011.9 or (ID 20240000059): This HI absorber seems to have been first discovered by FASHI. There is no optical spectroscopic redshift in the previous literature. In the foreground is the Milky Way, which may interfere with detecting the optical counterpart.

FASHI J060801.90+450814.2 or (ID 20240000507): This HI absorber seems to have been first detected by FASHI. There is no further information about this object. In the foreground is the Milky Way, which may interfere with detecting the optical counterpart.

FASHI J032614.32+492357.3 or (ID 20240000078): : This HI absorber appears to have been first detected by FASHI. There is no optical spectroscopic redshift in the previous literature. In the foreground is the Milky Way, which may interfere with detecting the optical counterpart.

FASHI J024600.14+511458.1 or (ID 20240000512): This HI absorber seems to have been first discovered by FASHI. There is no further information about this object. In the foreground is the Milky Way, which may interfere with detecting the optical counterpart.

FASHI J044433.30+525213.5 or (ID 20240000007): This HI absorber seems to have been first detected by FASHI. There is no further information about this object. In the foreground is the Milky Way, which may interfere with detecting the optical counterpart.

FASHI J030630.87+541208.7 or (ID 20240000083): This HI absorber seems to have been first discovered by FASHI. There is no optical spectroscopic redshift in the previous literature. In the foreground is the Milky Way, which may interfere with detecting the optical counterpart.

FASHI J043636.25+542201.5 or (ID 20240000005): This HI absorber seems to have been first detected by FASHI. The HI line shows not only an absorption feature but also an emission line profile. The HI line shows a narrow absorption feature at the center of the broad emission line. There is no optical spectroscopic redshift in the previous literature.

FASHI J134440.84+555306.2 or (ID 20240000023): This HI absorber has been reported in detail by Geréb et al. (2015). In Figure 2 we can see that the line width is extremely broad with $W_{50} = 521.8 \pm 11.9 \text{ km s}^{-1}$ and the optical morphology shows a long tidal tail extending 40 kpc to the south (Iwasawa et al. 2011). This object is the host of an ongoing merger.

FASHI J125614.58+565222.9 or (ID 20240000513): HI absorption was reported by Heckman et al. (1978); Gallimore et al. (1999). The radio source belongs to the Seyfert 2 galaxy.

FASHI J085519.79+575155.5 or (ID 20240000515): This absorber has been reported in detail by Zwaan et al. (2015); Curran et al. (2016). The HI absorption line is very narrow and strong.

FASHI J162636.67+580849.8 or (ID 20240000472): This HI absorber seems to have been first discovered by FASHI. The HI line shows not only an absorption feature but also an emission line profile. The HI line shows a narrow but strong absorption feature at the broad emission line center. There is no optical spectroscopic redshift in the previous literature.

FASHI J112832.57+583323.0 or (ID 20240000016): This absorber was reported by Dickey (1986); Baan & Haschick (1990). The HI line shows not only an absorption feature but also an emission line profile. The interaction system IC 694/NGC 3690 (Arp 299-Mrk 171) has been studied in HI absorption and OH emission with the VLA in the A configuration (Baan & Haschick 1990). The HI line shows not only an absorption feature but also an emission profile (see Figure 2). The emission component may come from the nearby interacting galaxy.

FASHI J114852.43+592501.9 or (ID 20240000471): This absorber was reported by [van Gorkom et al. \(1989\)](#); [Dickey \(1986\)](#); [Peck & Taylor \(2000\)](#). This galaxy is classified as elliptical by [de Vaucouleurs et al. \(1976\)](#) and as SO by [Nilson \(1973\)](#). The galaxy has a close binary SO companion, NGC 3895 ([van Gorkom et al. 1989](#)). The HI line shows not only an absorption feature but also an emission line profile. The HI emission component at $\sim 3500 \text{ km s}^{-1}$ may originate from the nearby galaxy (see [Figure 2](#)).

B. FIGURES ON INDIVIDUAL SOURCES

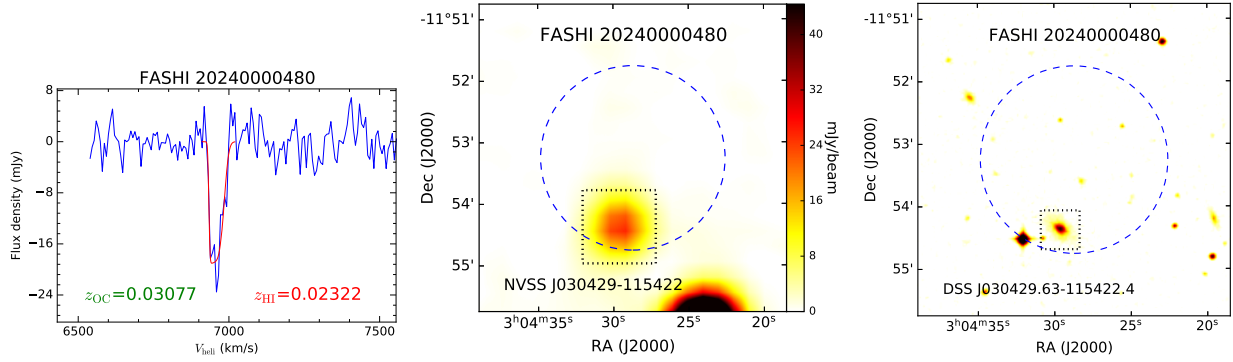


Figure 2 (Continued). 21 cm H I absorption galaxy FASHI 030428.71-115315.1 or ID 20240000480.

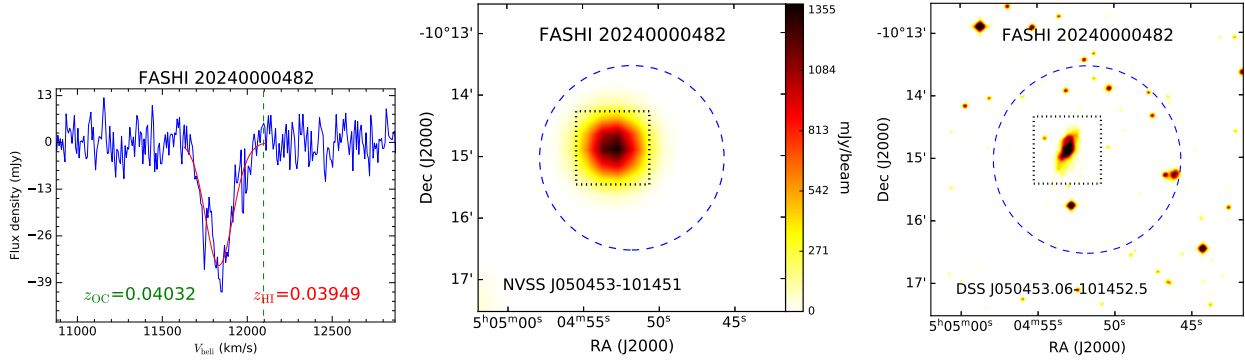


Figure 2 (Continued). 21 cm H I absorption galaxy FASHI 050451.78-101501.7 or ID 20240000482.

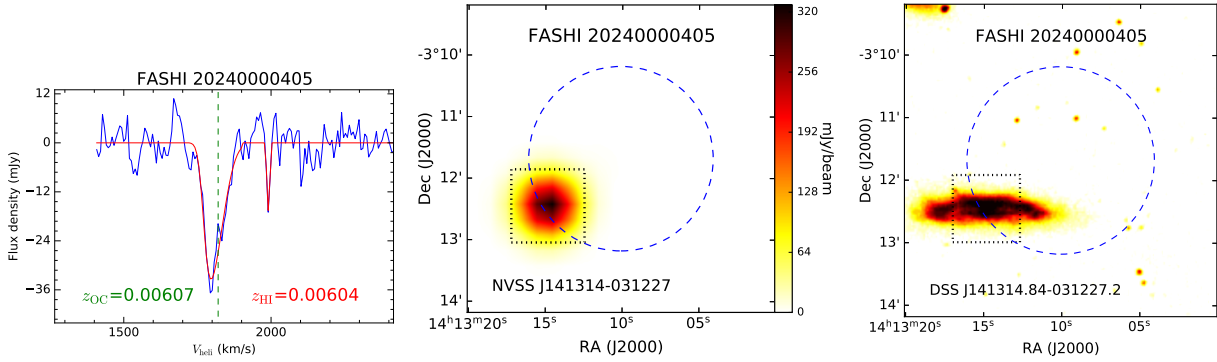


Figure 2 (Continued). 21 cm H I absorption galaxy FASHI 141310.09-031140.8 or ID 20240000405.

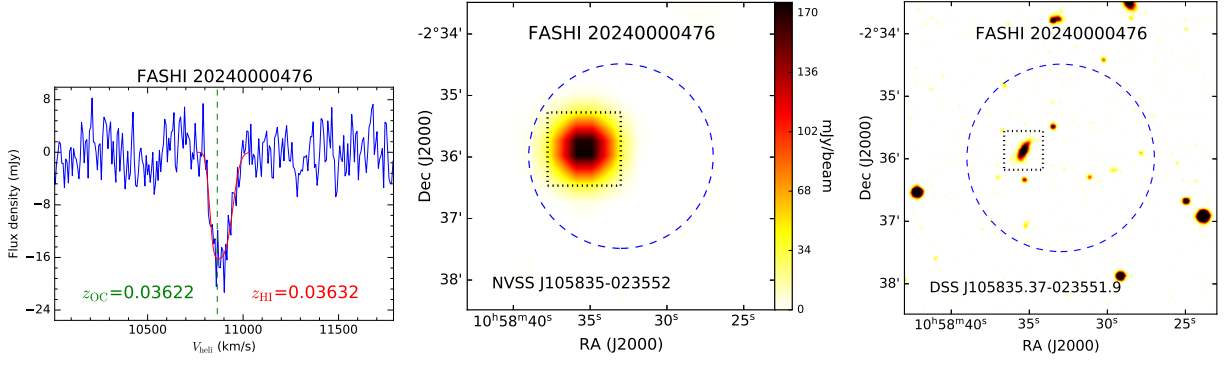


Figure 2 (Continued). 21 cm H I absorption galaxy FASHI 105833.00-023559.1 or ID 20240000476.

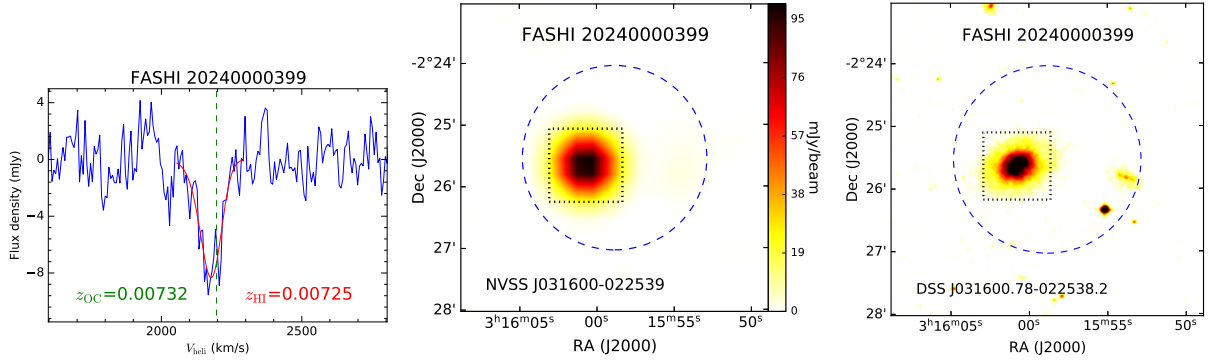


Figure 2 (Continued). 21 cm H I absorption galaxy FASHI 031558.84-022532.1 or ID 20240000399.

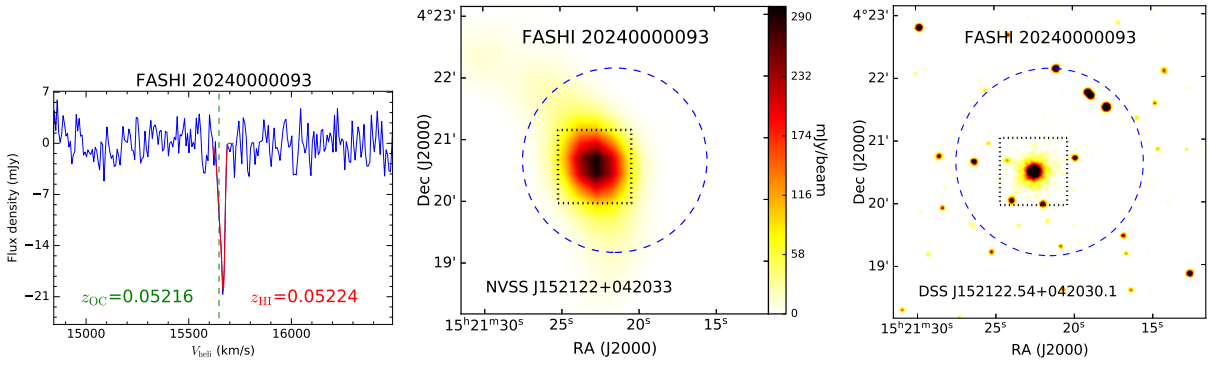


Figure 2 (Continued). 21 cm H I absorption galaxy FASHI 152121.51+042039.1 or ID 20240000093.

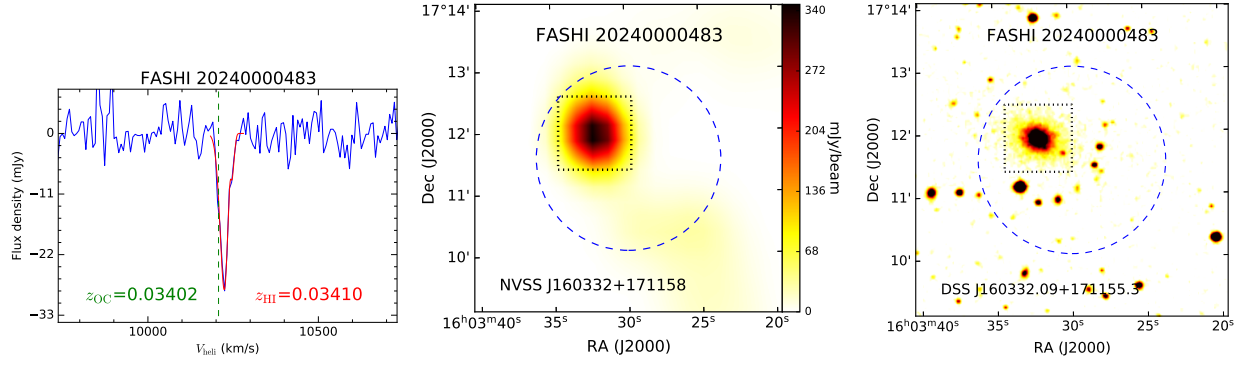


Figure 2 (Continued). 21 cm HI absorption galaxy FASHI 160329.87+171133.9 or ID 20240000483.

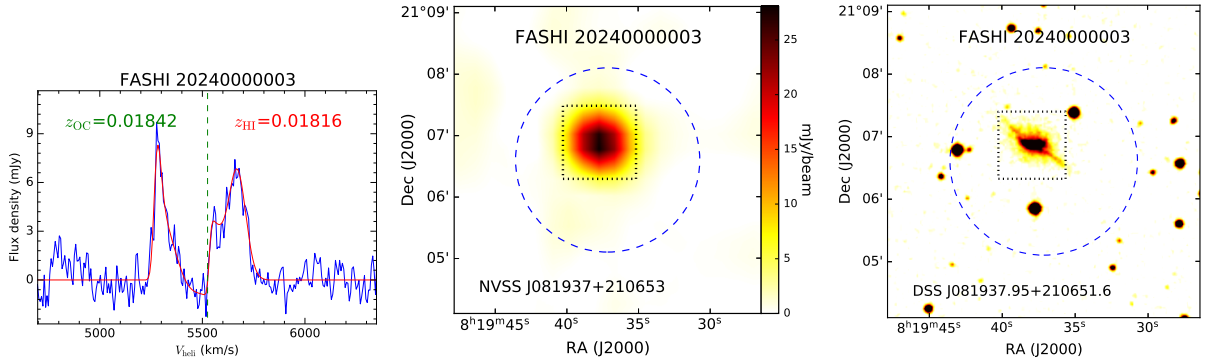


Figure 2 (Continued). 21 cm HI absorption galaxy FASHI 081937.14+210636.1 or ID 20240000003.

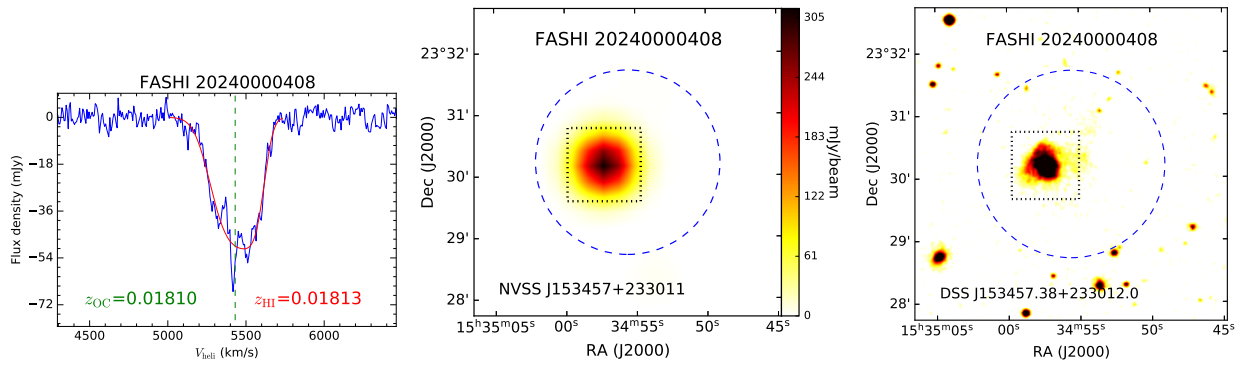


Figure 2 (Continued). 21 cm HI absorption galaxy FASHI 153455.59+233013.2 or ID 20240000408.

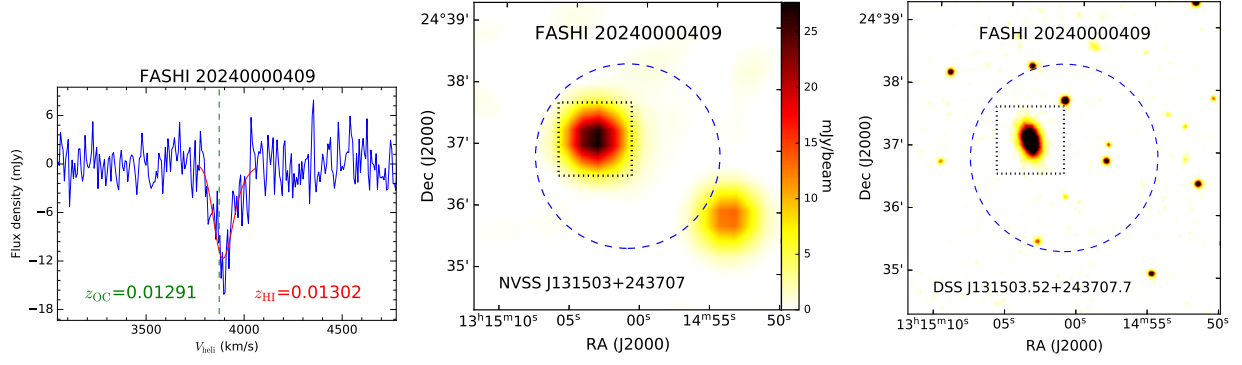


Figure 2 (Continued). 21 cm HI absorption galaxy FASHI 131501.12+243651.4 or ID 20240000409.

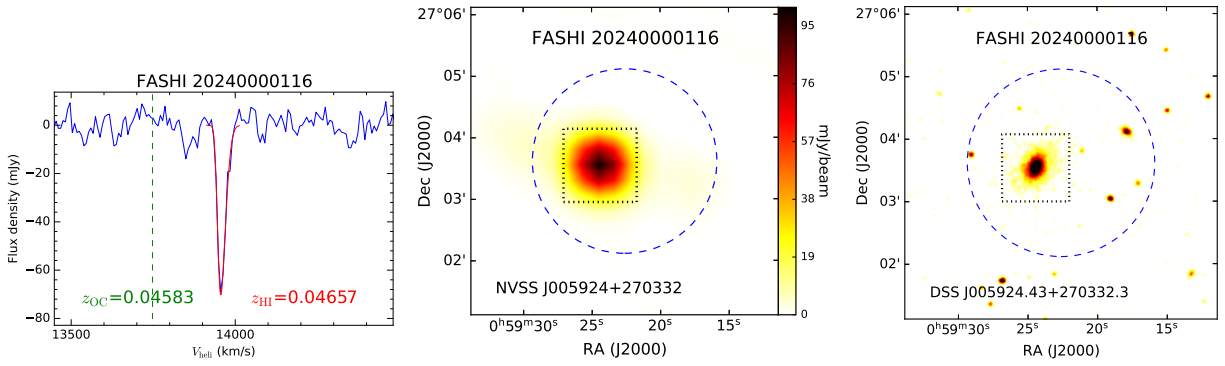


Figure 2 (Continued). 21 cm HI absorption galaxy FASHI 005922.61+270337.1 or ID 20240000116.

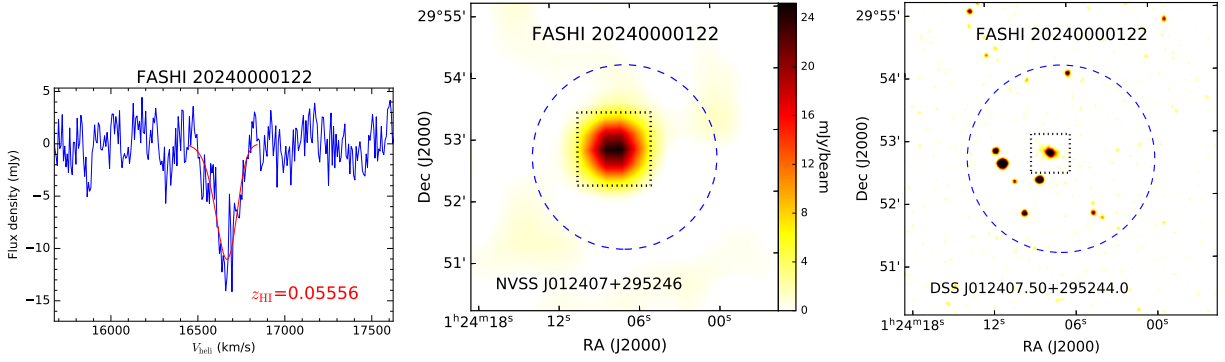


Figure 2 (Continued). 21 cm HI absorption galaxy FASHI 012406.73+295238.5 or ID 20240000122.

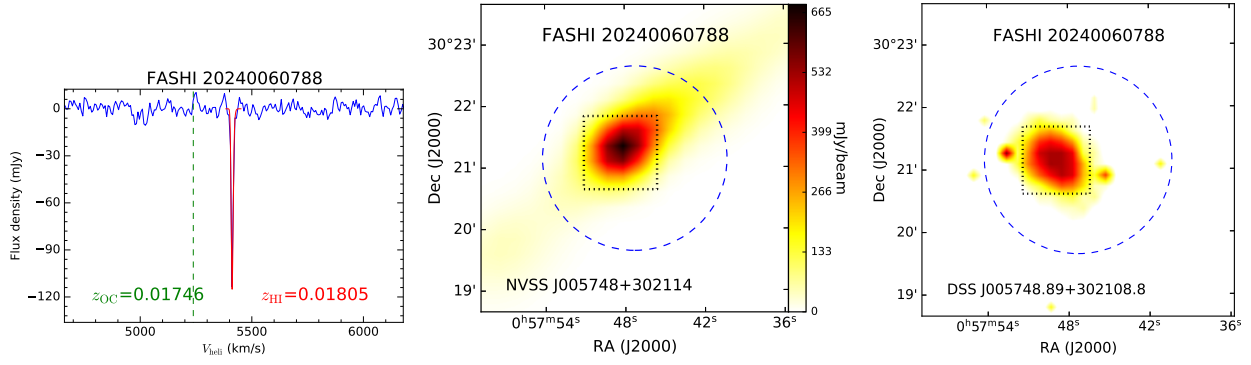


Figure 2 (Continued). 21 cm HI absorption galaxy FASHI 005747.27+302108.9 or ID 20240060788.

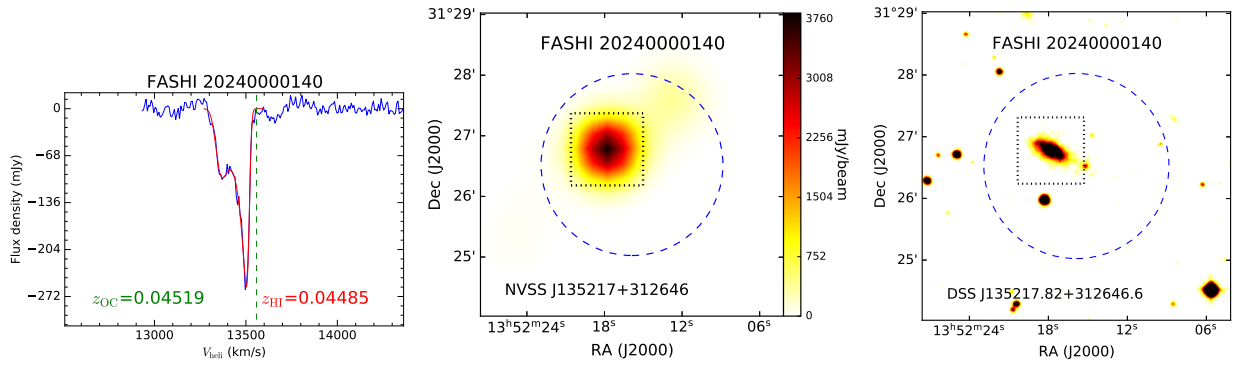


Figure 2 (Continued). 21 cm HI absorption galaxy FASHI 135215.88+312631.6 or ID 20240000140.

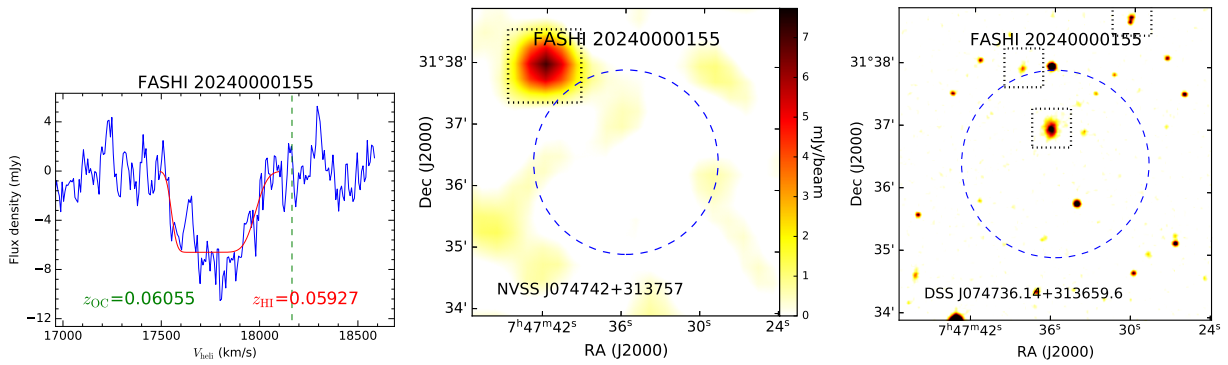


Figure 2 (Continued). 21 cm HI absorption galaxy FASHI 074735.82+313625.2 or ID 20240000155.

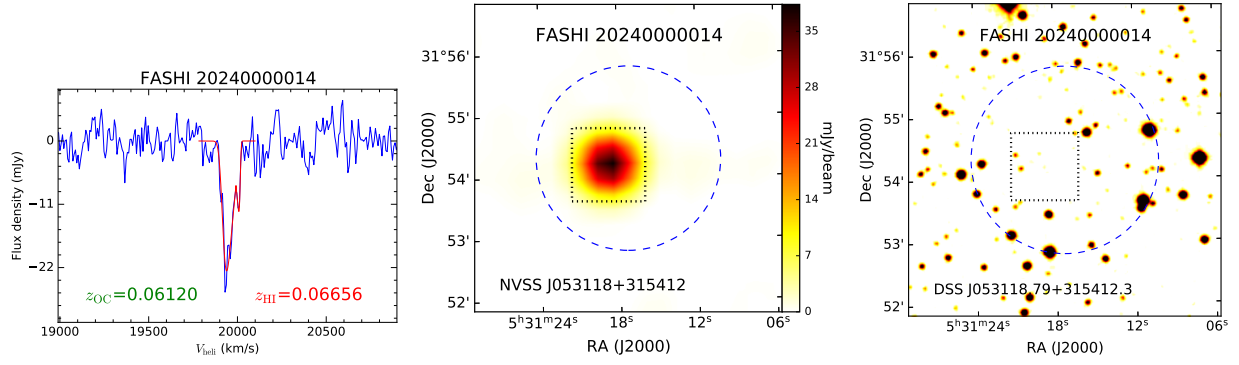


Figure 2 (Continued). 21 cm H I absorption galaxy FASHI 053117.26+315418.4 or ID 20240000014.

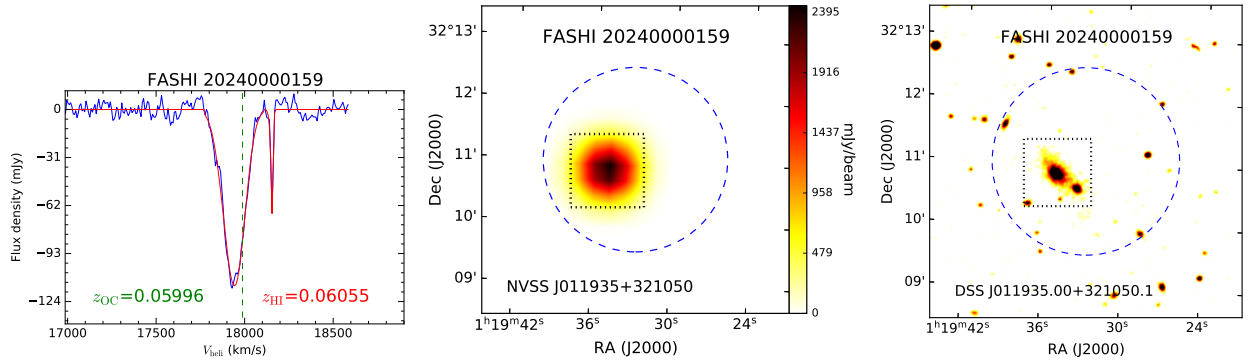


Figure 2 (Continued). 21 cm H I absorption galaxy FASHI 011932.90+321101.9 or ID 20240000159.

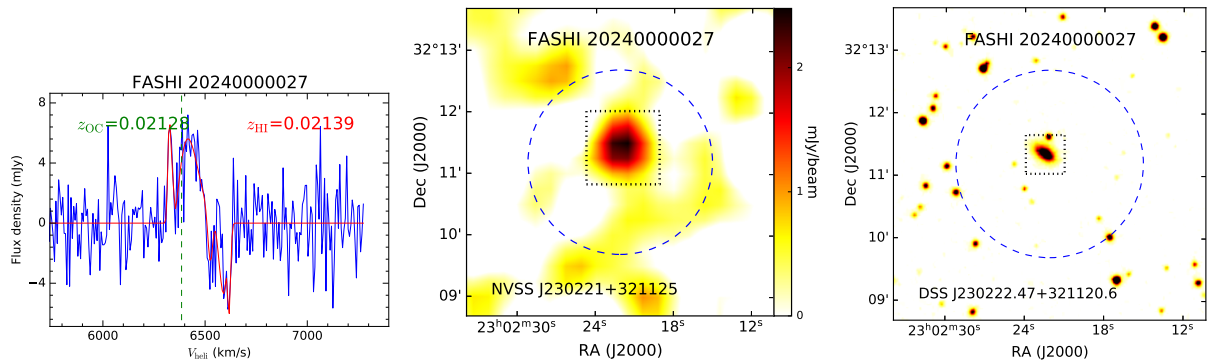


Figure 2 (Continued). 21 cm H I absorption galaxy FASHI 230222.13+321111.5 or ID 20240000027.

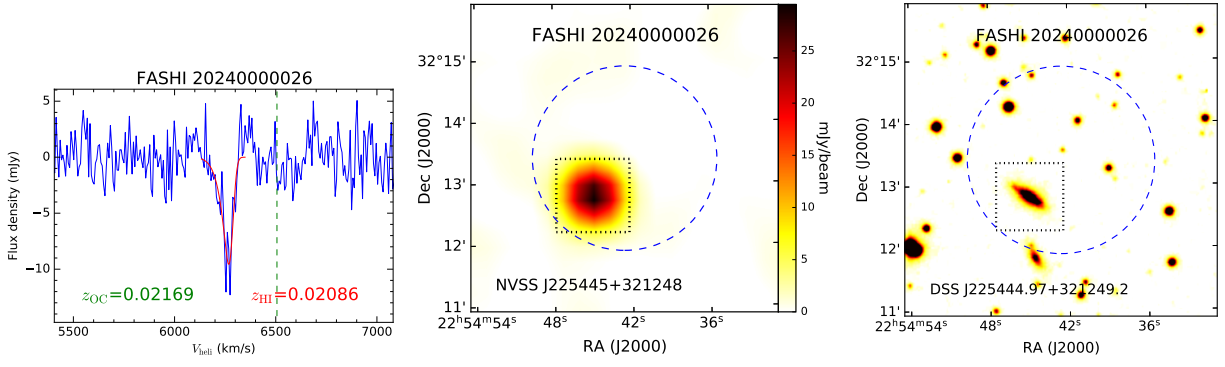


Figure 2 (Continued). 21 cm HI absorption galaxy FASHI 225442.56+321324.2 or ID 20240000026.

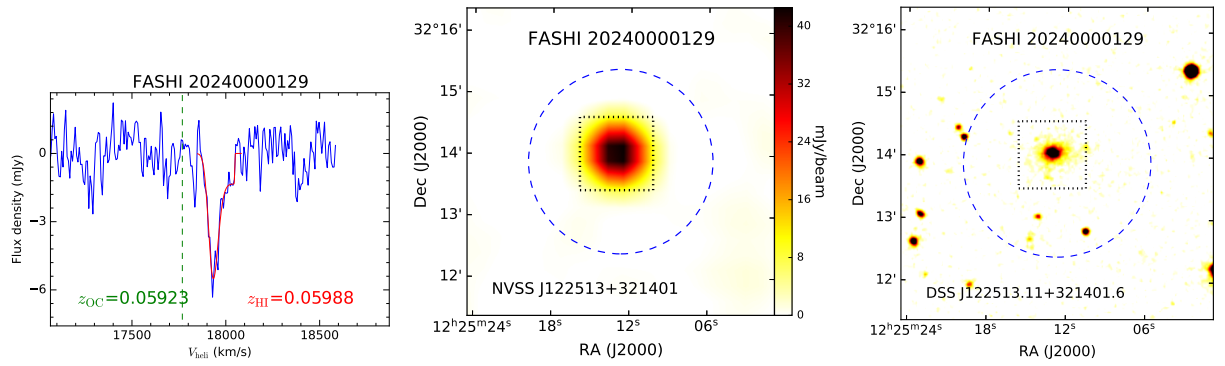


Figure 2 (Continued). 21 cm HI absorption galaxy FASHI 122512.74+321353.4 or ID 20240000129.

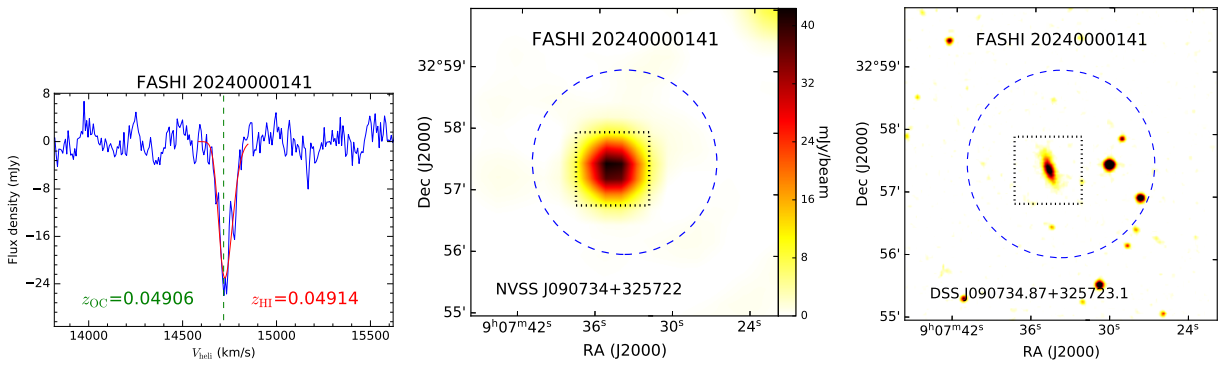


Figure 2 (Continued). 21 cm HI absorption galaxy FASHI 090733.90+325729.4 or ID 20240000141.

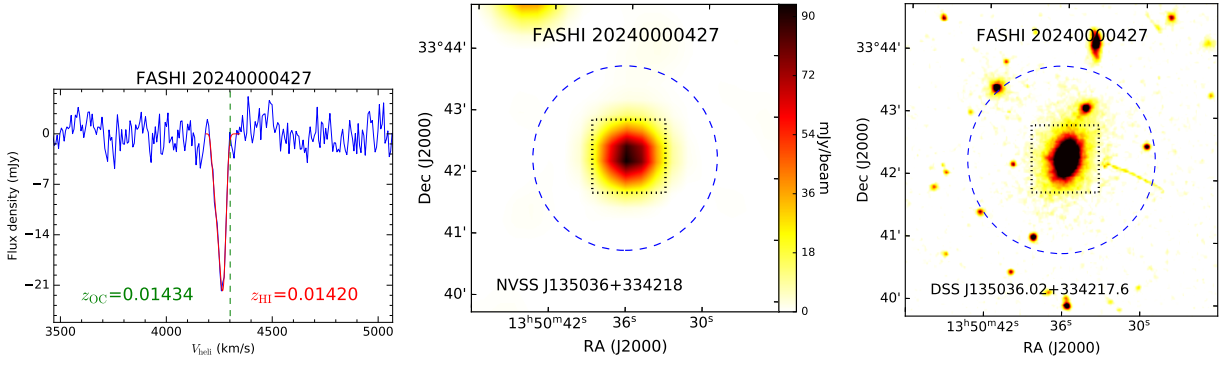


Figure 2 (Continued). 21 cm H I absorption galaxy FASHI 135036.30+334216.5 or ID 20240000427.

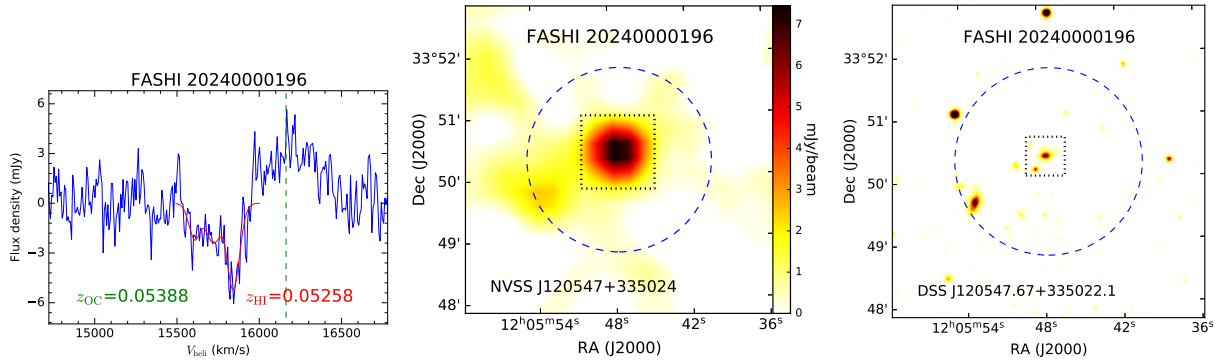


Figure 2 (Continued). 21 cm H I absorption galaxy FASHI 120547.43+335016.9 or ID 20240000196.

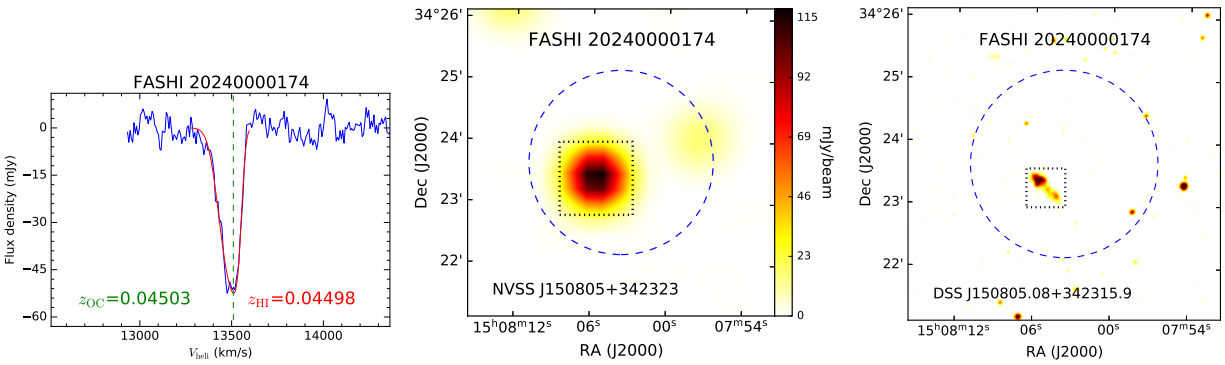


Figure 2 (Continued). 21 cm H I absorption galaxy FASHI 150803.69+342339.2 or ID 20240000174.

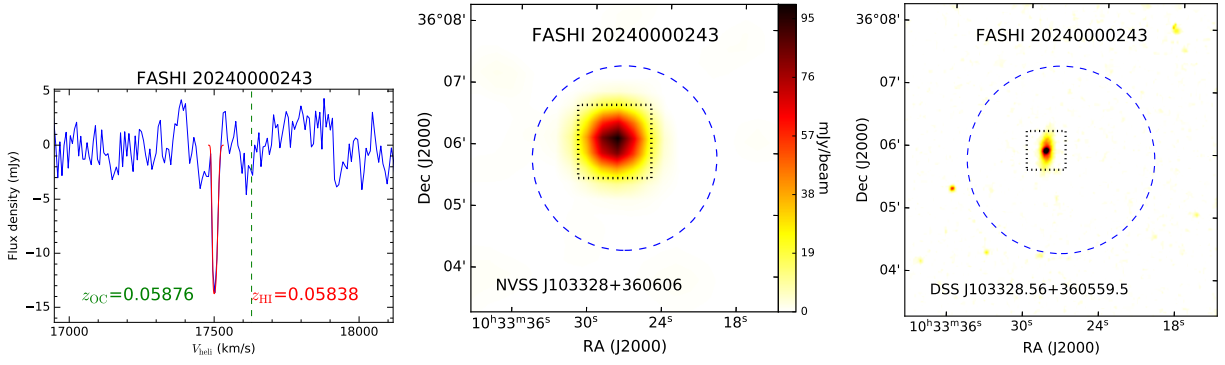


Figure 2 (Continued). 21 cm HI absorption galaxy FASHI 103327.36+360550.9 or ID 20240000243.

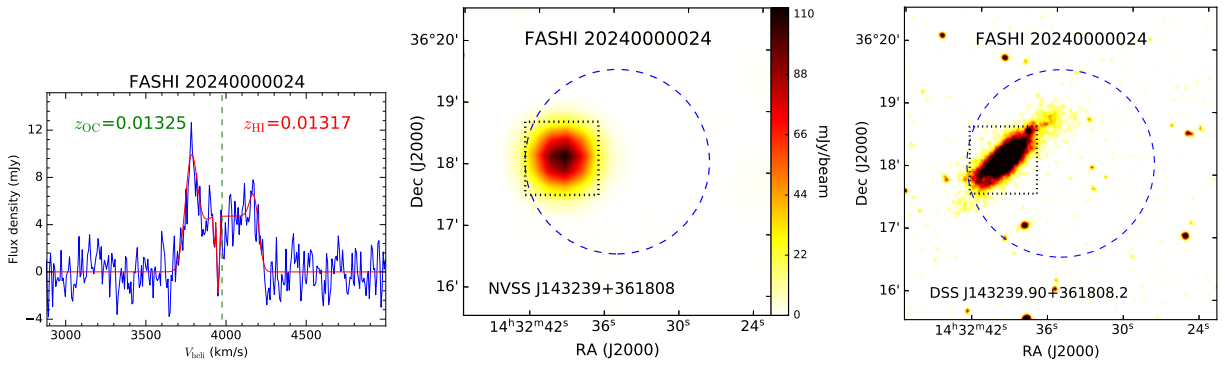


Figure 2 (Continued). 21 cm HI absorption galaxy FASHI 143235.35+361806.7 or ID 20240000024.

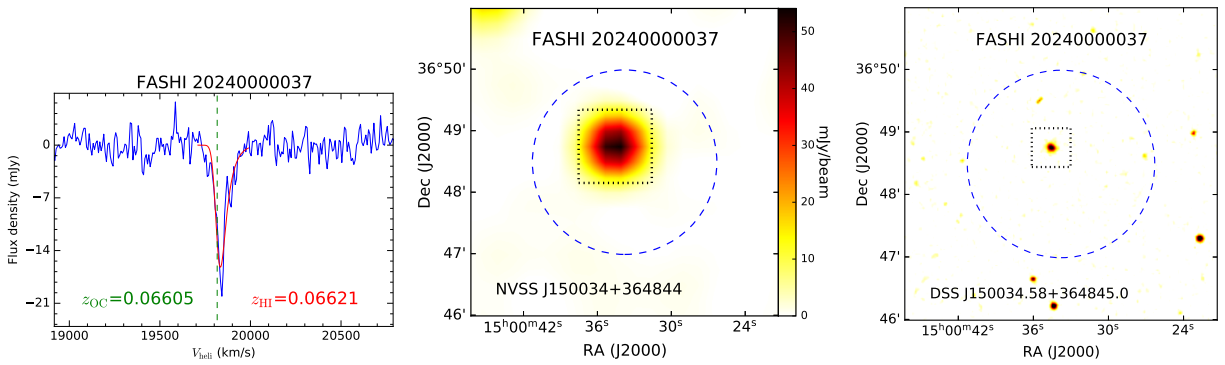


Figure 2 (Continued). 21 cm HI absorption galaxy FASHI 150033.79+364829.3 or ID 20240000037.

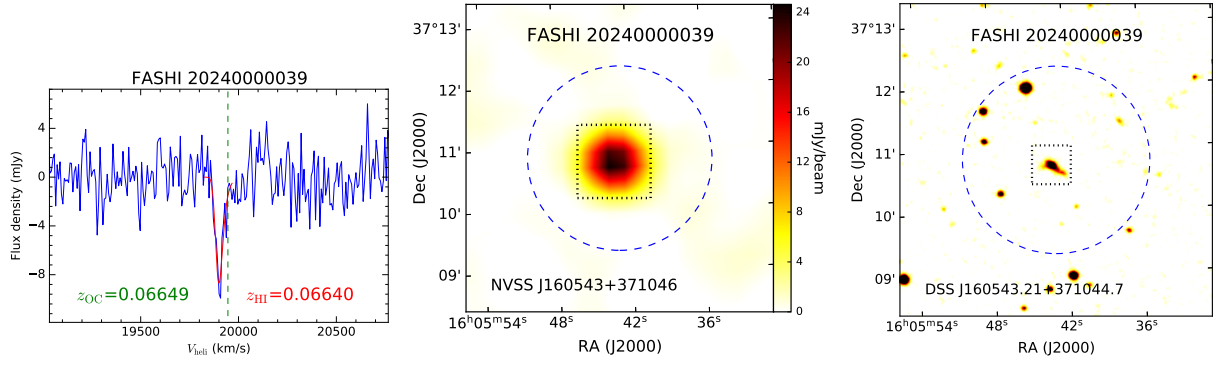


Figure 2 (Continued). 21 cm HI absorption galaxy FASHI 160542.81+371049.2 or ID 20240000039.

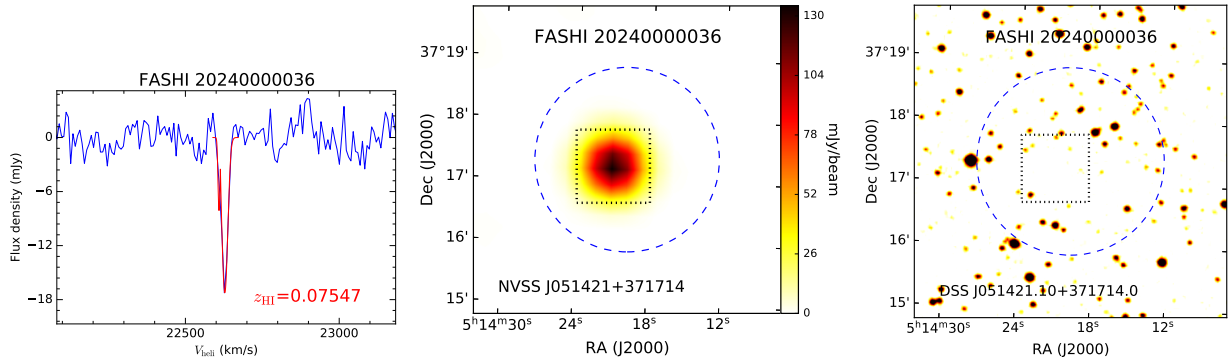


Figure 2 (Continued). 21 cm HI absorption galaxy FASHI 051419.90+371721.2 or ID 20240000036.

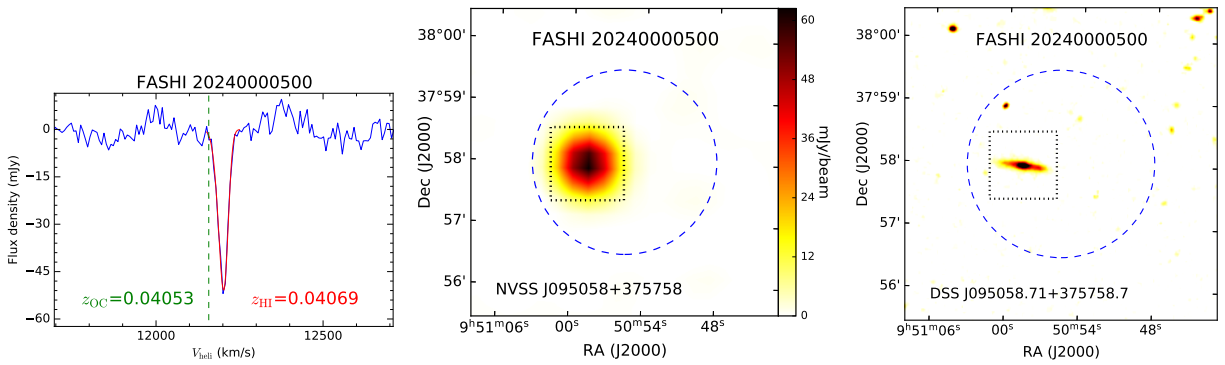


Figure 2 (Continued). 21 cm HI absorption galaxy FASHI 095055.65+375800.8 or ID 20240000500.

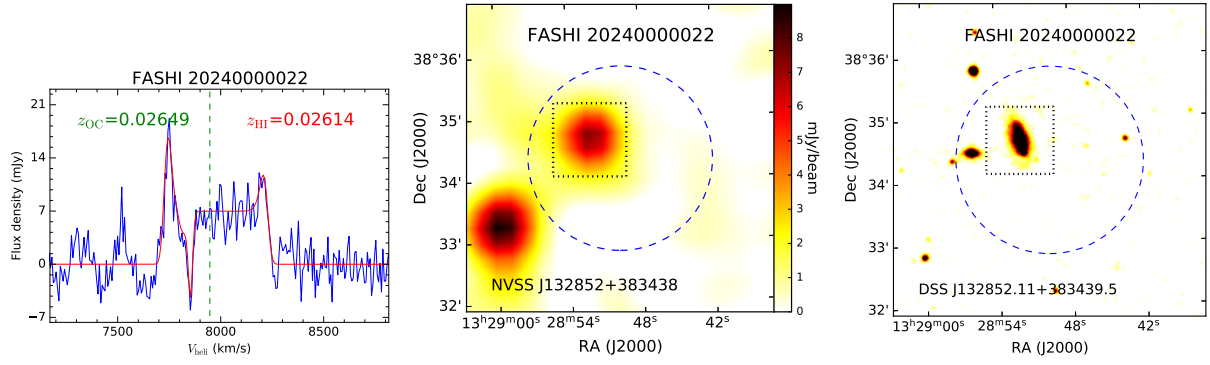


Figure 2 (Continued). 21 cm HI absorption galaxy FASHI 132849.73+383419.9 or ID 2024000022.

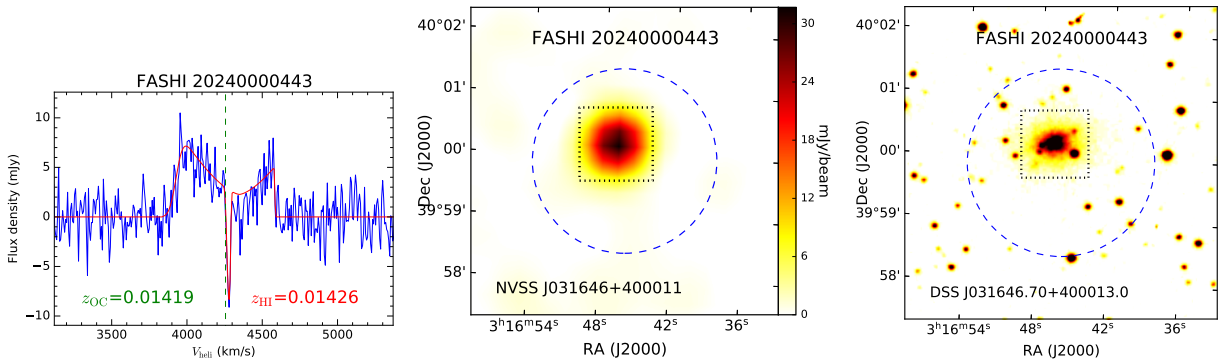


Figure 2 (Continued). 21 cm HI absorption galaxy FASHI 031646.12+395955.4 or ID 20240000443.

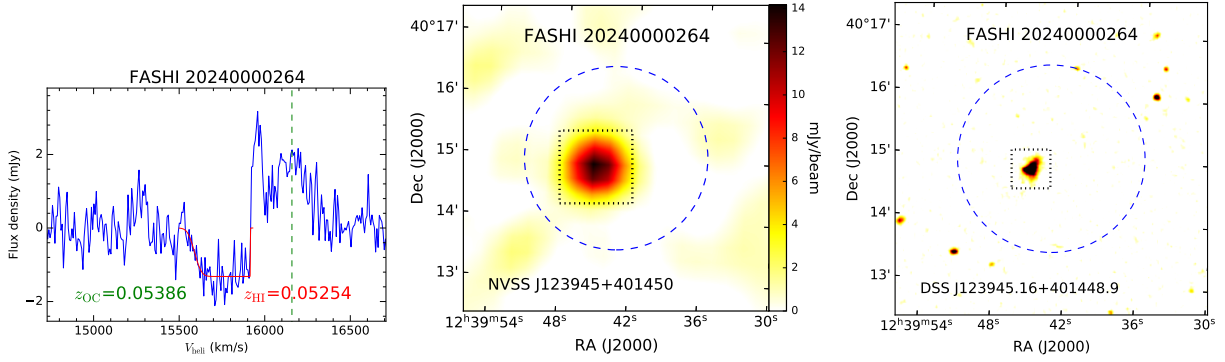


Figure 2 (Continued). 21 cm HI absorption galaxy FASHI 123943.52+401459.7 or ID 20240000264.

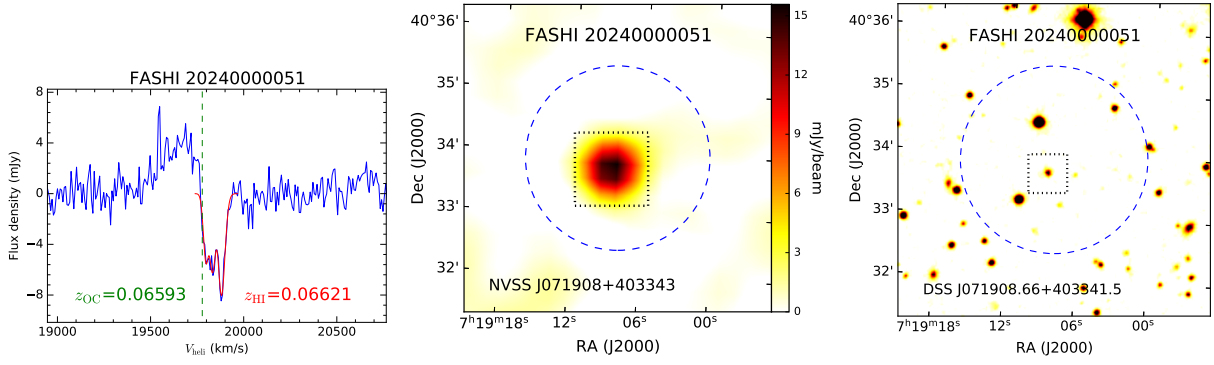


Figure 2 (Continued). 21 cm H I absorption galaxy FASHI 071908.19+403355.0 or ID 20240000051.

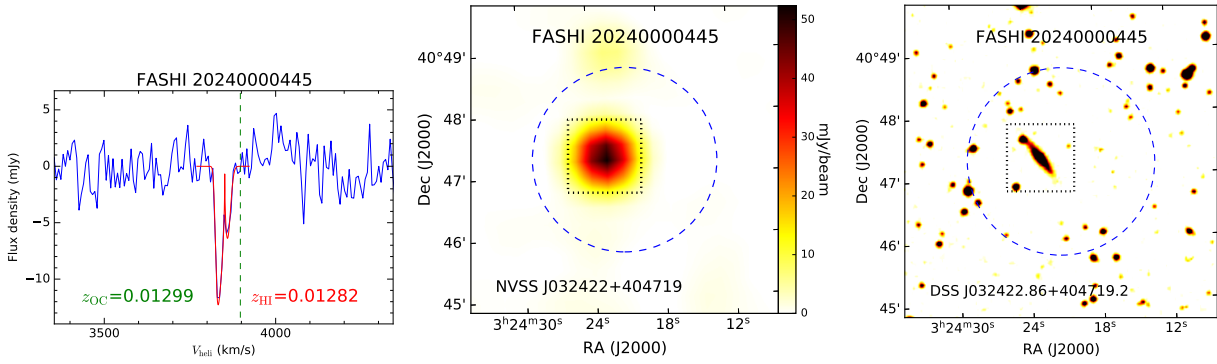


Figure 2 (Continued). 21 cm H I absorption galaxy FASHI 032421.15+404714.8 or ID 20240000445.

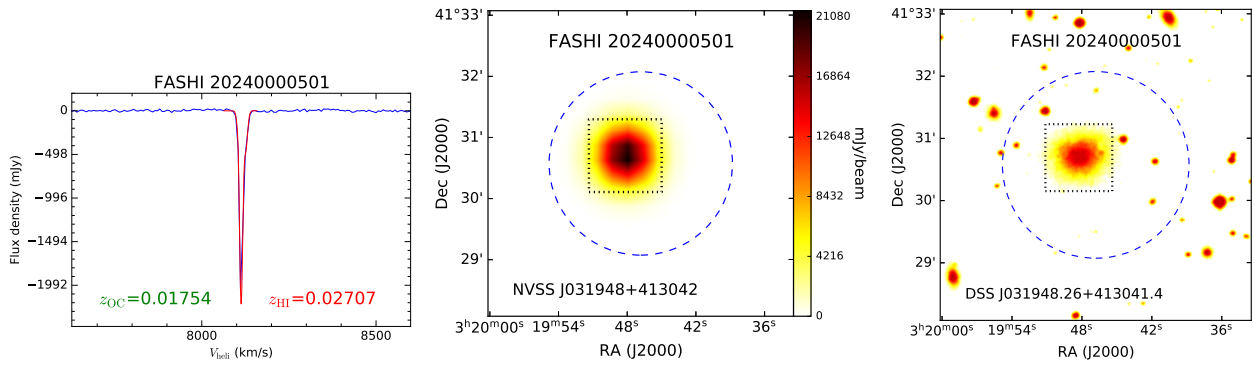


Figure 2 (Continued). 21 cm H I absorption galaxy FASHI 031946.81+413034.4 or ID 20240000501.

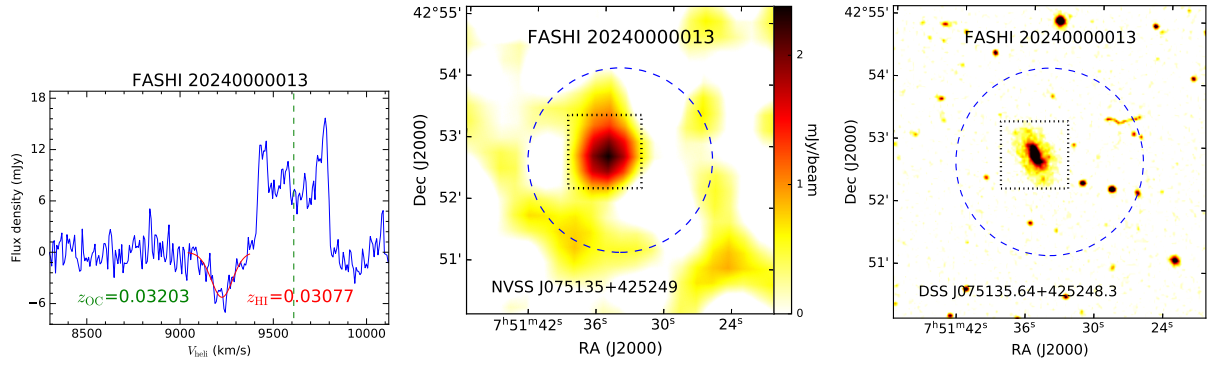


Figure 2 (Continued). 21 cm HI absorption galaxy FASHI 075134.30+425242.1 or ID 20240000013.

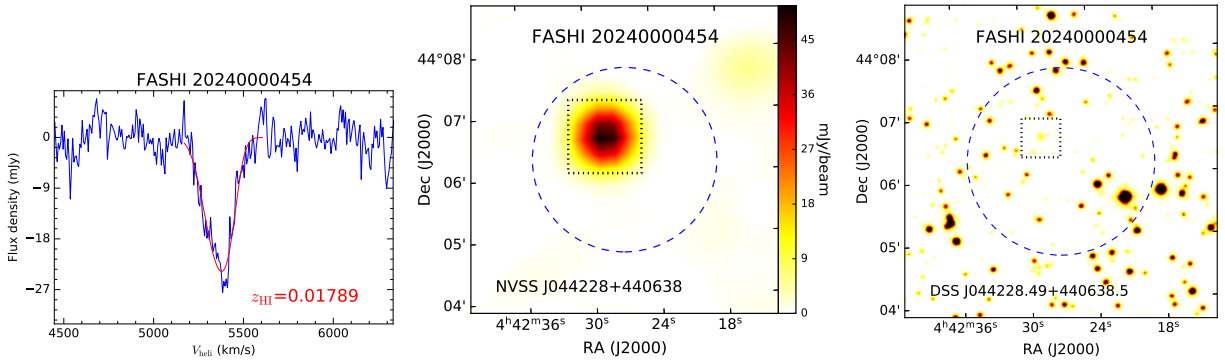


Figure 2 (Continued). 21 cm HI absorption galaxy FASHI 044226.82+440615.0 or ID 20240000454.

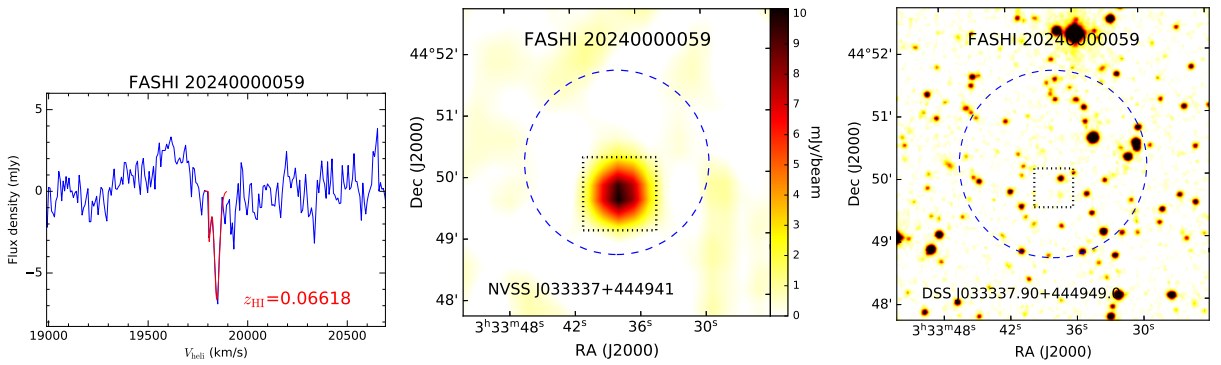


Figure 2 (Continued). 21 cm HI absorption galaxy FASHI 033337.92+445011.9 or ID 20240000059.

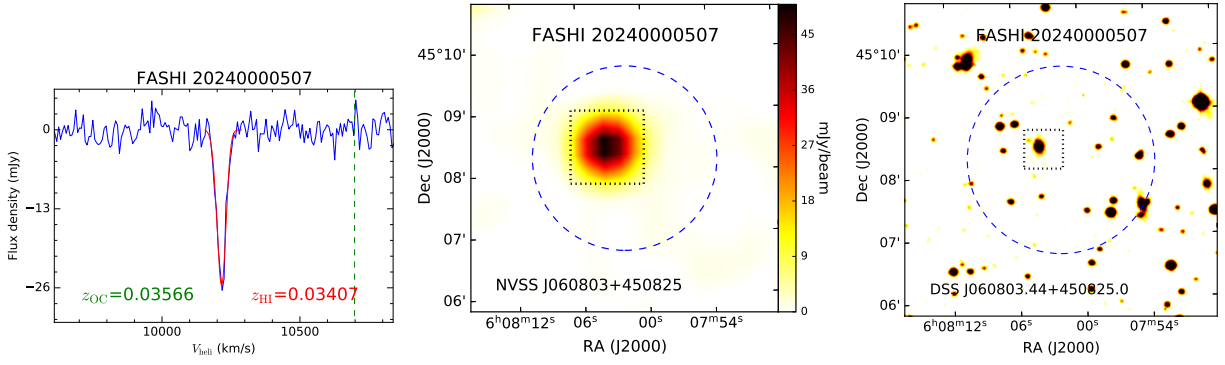


Figure 2 (Continued). 21 cm H I absorption galaxy FASHI 060801.90+450814.2 or ID 20240000507.

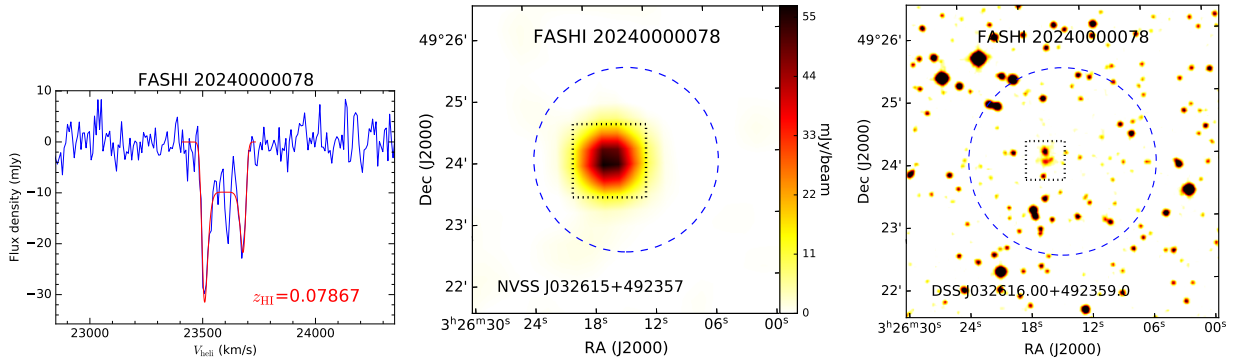


Figure 2 (Continued). 21 cm H I absorption galaxy FASHI 032614.32+492357.3 or ID 20240000078.

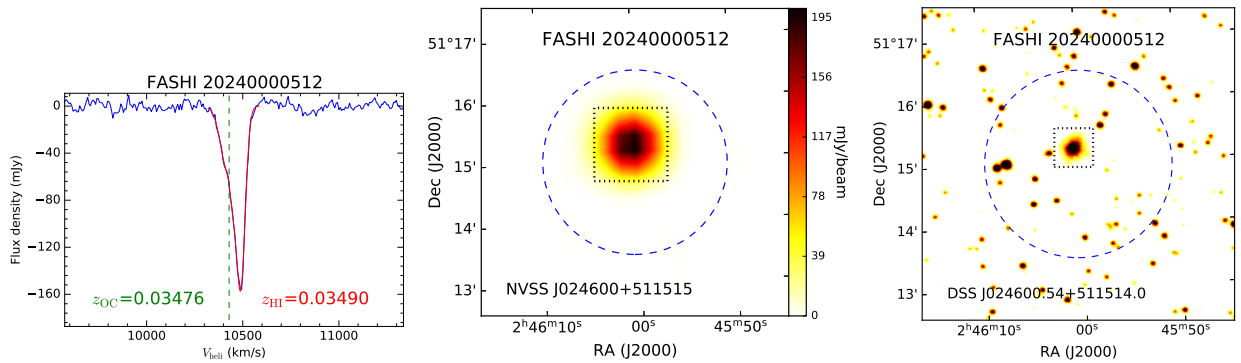


Figure 2 (Continued). 21 cm H I absorption galaxy FASHI 024600.14+511458.1 or ID 20240000512.

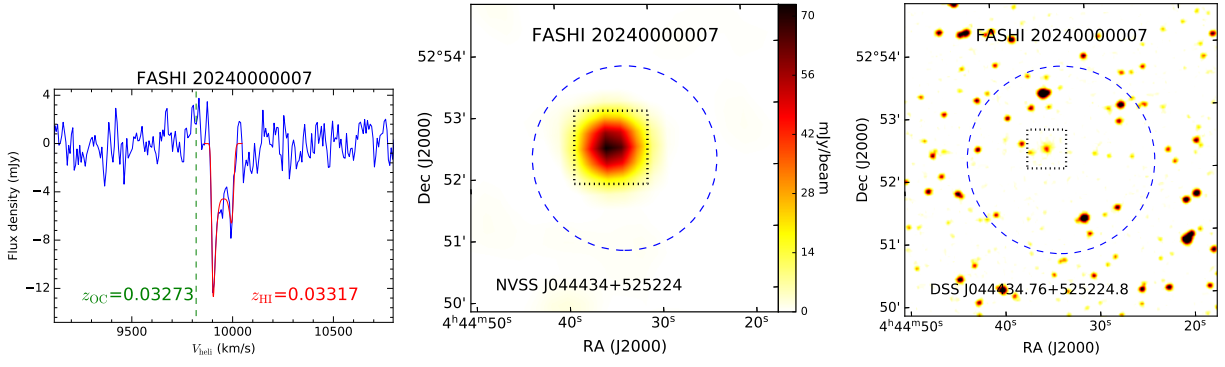


Figure 2 (Continued). 21 cm HI absorption galaxy FASHI 044433.30+525213.5 or ID 2024000007.

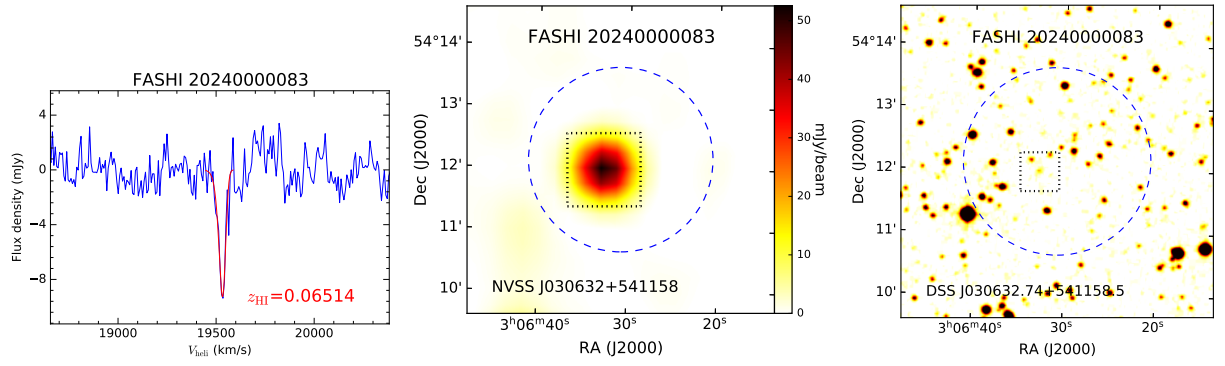


Figure 2 (Continued). 21 cm HI absorption galaxy FASHI 030630.87+541208.7 or ID 20240000083.

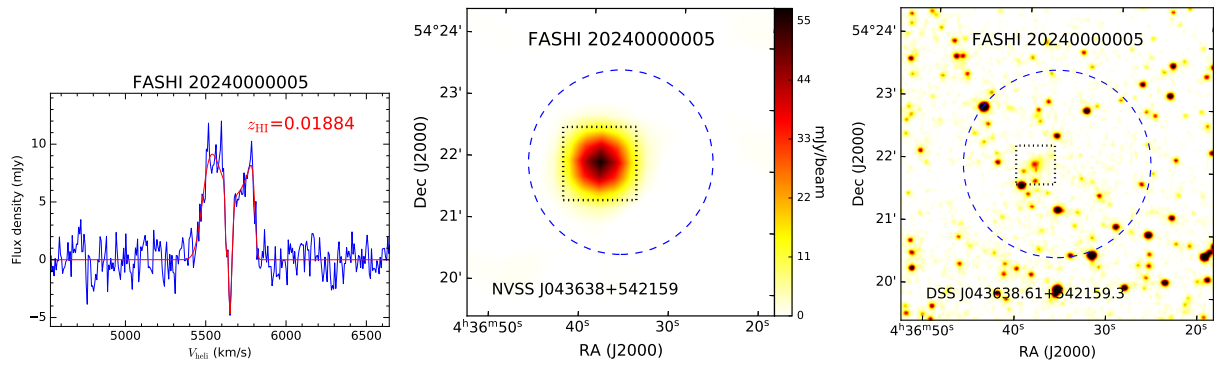


Figure 2 (Continued). 21 cm HI absorption galaxy FASHI 043636.25+542201.5 or ID 20240000005.

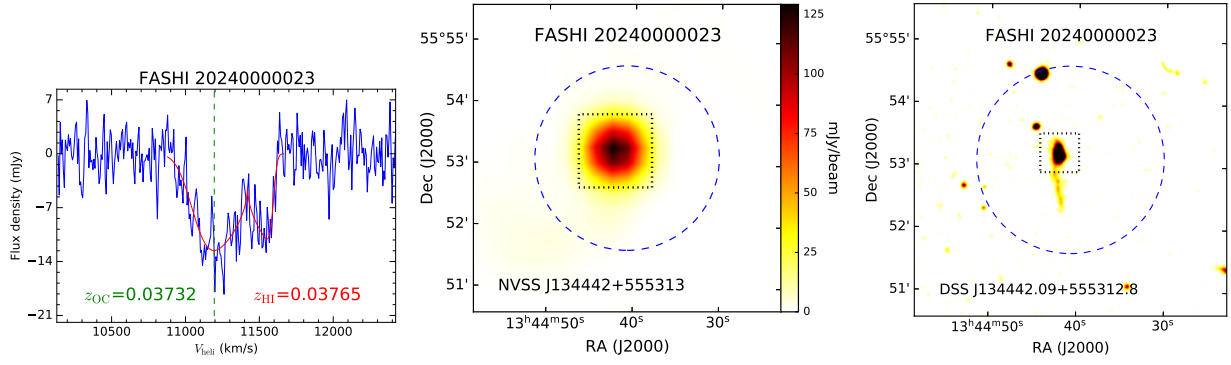


Figure 2 (Continued). 21 cm H I absorption galaxy FASHI 134440.84+555306.2 or ID 2024000023.

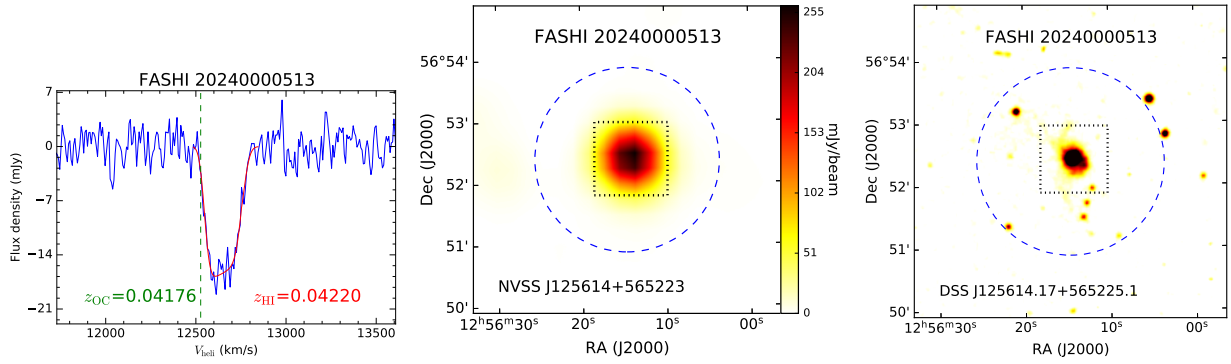


Figure 2 (Continued). 21 cm H I absorption galaxy FASHI 125614.58+565222.9 or ID 20240000513.

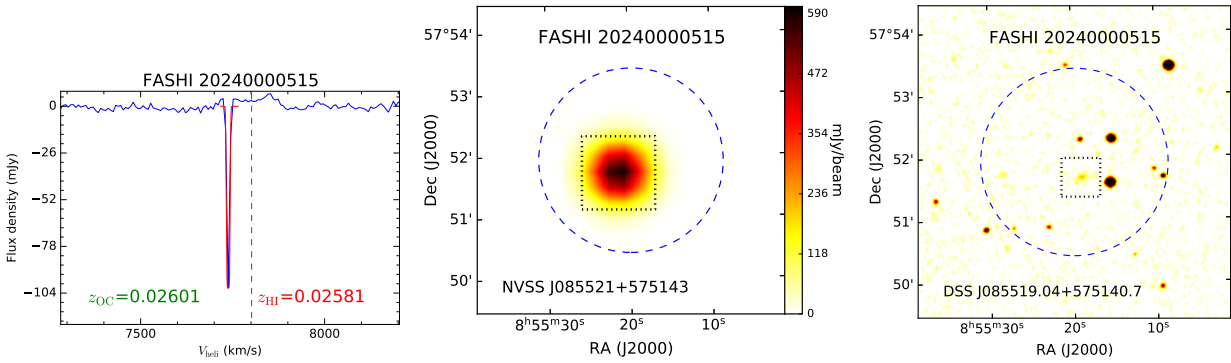


Figure 2 (Continued). 21 cm H I absorption galaxy FASHI 085519.79+575155.5 or ID 20240000515.

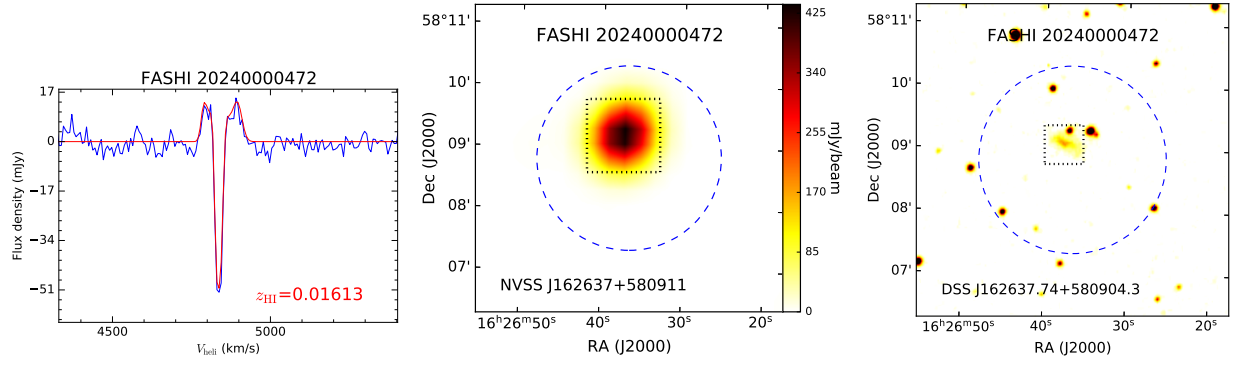


Figure 2 (Continued). 21 cm HI absorption galaxy FASHI 162636.67+580849.8 or ID 20240000472.

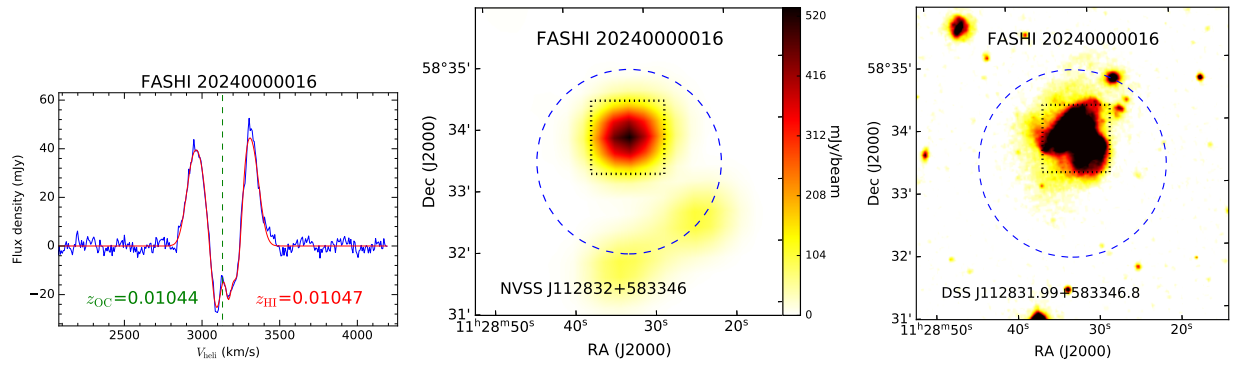


Figure 2 (Continued). 21 cm HI absorption galaxy FASHI 112832.57+583323.0 or ID 20240000016.

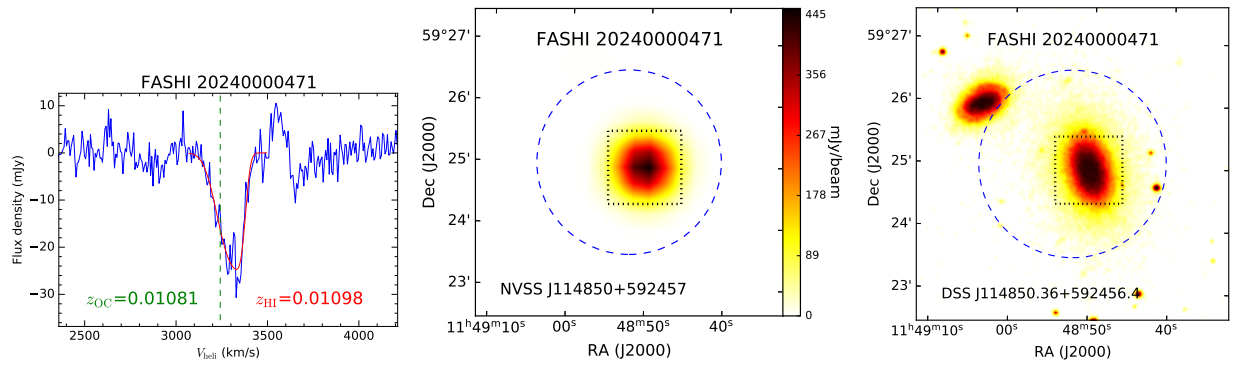


Figure 2 (Continued). 21 cm HI absorption galaxy FASHI 114852.43+592501.9 or ID 20240000471.